

# From Isolated Islands to *Pangea*: Unifying Semantic Space for Human Action Understanding

Yong-Lu Li\*, Xiaoqian Wu\*, Xinpeng Liu, Yiming Dou, Yikun Ji, Junyi Zhang, Yixing Li, Jingru Tan, Xudong Lu, Cewu Lu<sup>†</sup>  
 Shanghai Jiao Tong University

{yonglu\_li, enlighten, douyiming, junyizhang, lyxinguo, luxudong2001, lucewu}@sjtu.edu.cn,  
 {xinpengliu0907, jiyikun2002, tanjingru120}@gmail.com

## Abstract

Action understanding matters and attracts attention. It can be formed as the mapping from the action physical space to the semantic space. Typically, researchers built action datasets according to idiosyncratic choices to define classes and push the envelope of benchmarks respectively. Thus, datasets are incompatible with each other like “**Isolated Islands**” due to semantic gaps and various class granularities, e.g., do housework in dataset A and wash plate in dataset B. We argue that a more principled semantic space is an urgent need to concentrate the community efforts and enable us to use all datasets together to pursue generalizable action learning. To this end, we design a **Poincaré action semantic space** given verb taxonomy hierarchy and covering massive actions. By aligning the classes of previous datasets to our semantic space, we gather (image/video/skeleton/MoCap) datasets into a unified database in a unified label system, i.e., bridging “isolated islands” into a “**Pangea**”. Accordingly, we propose a bidirectional mapping model between physical and semantic space to fully use Pangea. In extensive experiments, our system shows significant superiority, especially in transfer learning. **Code and data will be publicly available at** <https://mvig-rhos.com/pangea>.

## 1. Introduction

Visual action understanding is an important direction in computer vision and matters to various domains [1, 2]. Generally speaking, it can be formulated as the mapping from the physical space to the semantic space. Here, **physical** space indicates the visual patterns (information carrier) and **semantic** space represents the action semantics (class).

\*The first two authors contribute equally.

<sup>†</sup>Corresponding author.

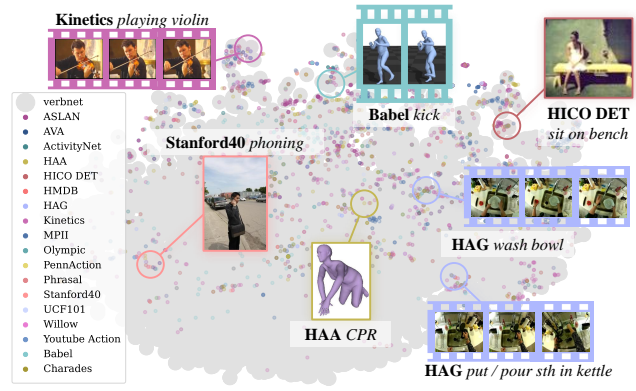


Figure 1: “Isolated islands”. The semantic gap brings a great challenge to general action understanding.

In terms of the physical space, many works were proposed to extract representations from different modalities to capture action cues, such as image [3], video [4], skeleton [5], MoCap [6], RGBD [7], etc. However, few efforts have been made to semantic space design. Previous benchmarks [8, 9, 10] are typically designed according to designers’ choice and incompatible with each other due to semantic gaps. They have three main weaknesses: (1) **Ambiguity**. Similar actions may have different class names, e.g., clean, wipe, scrub. Though this may strengthen the diversity in visual-language learning [11], it hinders machines learn the subtle similarity and differences of actions. Besides, the same class may represent different actions, e.g., address means either addressing oneself to something or addressing a conference. This phenomenon brings both generalization possibility and challenge. (2) Overlooking **granularity/hierarchy**. The datasets are constructed independently, thus typically overlooking granularity, e.g., do housework in dataset A and clean floor in dataset B, sometimes even in one dataset. (3) **Integration/transfer difficulty**. Large models need more data. However, due to the “isolated islands”, it is hard to integrate datasets and

conclude the “few-shotness” and “zero-shotness” of classes. We do not know which classes should be enriched or used for transfer learning.

In Fig. 1, we visualize the class word embeddings [12] of 18 datasets via t-SNE. Huge semantic gaps exist. Even for the very large Kinetics-700 [4], there are still many classes beyond its coverage. Here, we first clearly reveal the overlooked “**Isolated Islands** ( $I^2$ )” problem. It brings semantic gaps and impedes cross-dataset learning. Though CLIP [11] like works alleviate this problem to some extent with the open-vocabulary property, their latent space may be difficult to capture the subtle *polysemy*, *taxonomy*, and *hierarchy* of action semantics. In experiments (Sec. 6), CLIP trained with simply-mixed datasets performs not well.

Thus, we rethink the action semantic space design and take a step towards a principled semantic space. We propose a new system to pave a promising way to address the  $I^2$  problem. Our core idea is to use a **Poincaré action semantic space** to replace the existing hand-crafted ones. We build this semantic space according to the linguistic structure knowledge of VerbNet [13]. VerbNet is a network linking the syntactic and semantic patterns of verbs. It is a domain-independent tree-structure lexicon and has a clear hierarchy covering most verbs. We visualize the verb tree in Fig. 2.

To maximize the potential of our semantic space, we gather many datasets (image/video/skeleton/MoCap) to build a database and align their classes to our semantic space easily. That is, linking the “isolated islands” into a “**Pangea**”. Then, we can use a continuous Poincaré ball together with the semantic-geometric prompt to embed the structured knowledge.

Our space has four-fold superiority: (1) **Unambiguous** verb nodes correlating all related verbs, *e.g.*, *pat*, *nudge*, *massage* with similar meaning are shared by the node *touch-20-1*. (2) **Rich knowledge**. Besides the thematic role, syntactic, semantic description, and selectional preferences of verbs, VerbNet has mappings to other knowledge bases (WordNet [14], PropBank [15], FrameNet [16]). We can conveniently adopt Large Language Models [17] to extract meaningful language representations to advance learning. (3) **Hierarchy** to represent actions from abstract to specific granularity, *e.g.*, *sports*, *ball sports*, *basketball*, *dunk*. (4) **Extensive coverage**. It contains about **5,800** verbs. In Fig. 1, our space not only covers all datasets but also spans the semantics a lot.

To fully use *Pangea*, we also propose a *bidirectional mapping system* to conduct both action discrimination (bottom-up) and generation (top-down). It can map multi-modal physical patterns to the structured semantic space or inversely generate 3D motions. In experiments, our method armed with *Pangea* demonstrates representative and trans-

fer ability. On multi-modal benchmarks, it brings significant improvements. Besides, it can generate diverse and accurate 3D motions given single/compositional verb nodes.

Our contributions are three-fold: 1) We propose a structured semantic space to bridge the “isolated islands”. 2) We build the *Pangea* database gathering 28 multi-modal datasets. 3) A bidirectional system is proposed to conduct both action recognition and generation based on *Pangea*.

## 2. Related Work

**Action Understanding** has achieved progress recently. There are mainly image [8, 18, 19], video [20, 10, 21, 22, 23], skeleton [24], and 3D body [25] datasets. The common tasks are action recognition and temporal/spatial localization/detection. Early benchmarks focus on classifying an image or a short video into classes [21, 8, 19]. Recently, benchmarks that require both accurate recognition and active subject detection are emerging [20, 26, 27, 18, 28, 29, 30, 31]. Moreover, few/zero-shot action learning [32] also attracts attention. Many methods have been proposed to push this direction forward. For *image* tasks, 2D CNN is the dominant architecture, while knowledge like part state [33, 34, 35], 2D/3D human [36, 37, 38], and language prior [39, 40, 41, 3] are used too. For *video* tasks, 2D-CNN [42, 43, 44], two-stream network [45, 46], and 3D-CNN [4, 47] are the major architectures adopted. While for *skeleton* tasks, both GCN [48, 49, 50] and 2D-CNN [51, 52] are widely used. Recently, as the success of Transformer [53], besides directly importing it into action detection [54, 55], visual-language contrastive learning [11] has changed this direction a lot.

In terms of action semantic space, most datasets [8, 18, 20, 56, 57] overlook action hierarchy. While some works consider hierarchy [22, 58, 59]. For example, ActivityNet [22] defines 200+ action classes belong to 7 high-level classes (*e.g.*, *personal care*, *household*) based on activity scenarios; FineGym [58] organizes hierarchical actions from gymnasium videos; VerSe [60] augments COCO [61] and TUHOI [62] with verb sense labels to provide finer-grained action semantics on 3.5 K images. However, they are scale/class/domain-limited and built with manually-picked classes. Instead, we choose to cover the hierarchy based on well-defined linguistic works such as VerbNet [13], WordNet [14], FrameNet [16], *etc.*

**3D Action Generation** is an active field. With large skeleton datasets such as NTU [24] and Human3.6M [5], considerable efforts have been put on it [6, 63, 64, 65, 66]. While MoCap datasets [67, 6] push it further towards parametric human model-based generation [63]. Most efforts are either unconditional or conditioned on restricted action classes. Beyond class conditioned generation, some works conduct generation with natural language [64, 65] based on datasets composed of motion-text pairs [25, 68].

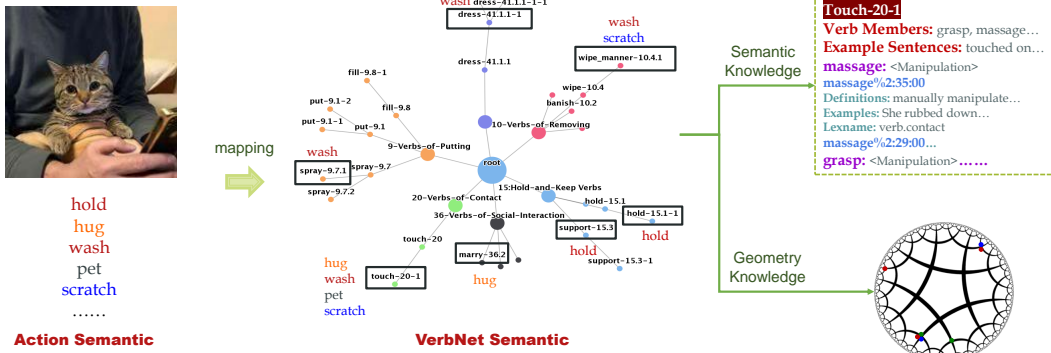


Figure 2: Verb tree. The conventional action semantics (e.g., hold, hug) can be mapped into node semantics (e.g., touch-20-1, support-15.3). The proposed semantic space has abundant semantic and geometry knowledge.

### 3. Preliminary

**Multi-Modal Physical Space.** We adopt two modalities for physical space  $P$ : 2D and 3D. For 2D, we adopt CNN or Transformer (e.g., ResNet [69], CLIP [11]) to extract representation from image/video. For 3D, we use the widely-used model SMPL [70] to embed 3D humans.

**Structured Semantic Space.** Intuitively, the ambiguity of objects is relatively smaller, thus objects/nouns are easier to label. Things are different for actions/verbs which are more ambiguous. Previous works typically design semantic space manually and optionally. Instead, we build the structured semantic space  $S$  via the hierarchical verb tree from VerbNet [13] (Fig. 2). Here, we define the *nodes* as the *classes* of our semantic space. Compared with conventional design [22], our space has elegant characteristics: (1) Due to the lack of a unified naming standard, classes of previous datasets have ambiguity. For example, different datasets may have feast, eating, and dining respectively, where a common semantic is shared. Instead, in our  $S$ , actions with **shared** meanings are connected with their **common** nodes. (2) Each node is equipped with **abundant knowledge**. In Fig. 2, “touch-20-1” node is explained by: a) Verb members, e.g., grasp; b) Example sentences as instantiations of the node semantics; c) Each verb member is explained via connections with other lexical resources (e.g., WordNet [14], FrameNet [16]). In Fig. 2, the verb massage is explained by its frame in FrameNet [16] (manipulation) and the corresponding items in WordNet [14] (“massage%2:35:00”, “massage%2:29:00”). (3) **Hierarchy** reveals semantic connections between nodes and provides structured knowledge. The nodes are numbered according to shared semantics and syntax. Nodes sharing a high-level number (9-109) have semantic relations [13], e.g., “banish-10.2” and “wipe-10.4” share a parent node as they are all about removing. Though some works [22, 58] consider hierarchy too, they are either of limited coverage or defined empirically according to scenes. Instead, our verb semantics are more explicit. (4) Our  $S$  covers **5,800+** verbs which is broader than previous works.

### 4. Constructing Pangea

**Data Curation.** With the structured  $S$ , we can collect data with diverse modalities, formats, and granularities, and adapt them into a unified form. Our database *Pangea* contains a large range of data including *image*, *video*, and *skeleton/MoCap*. We process and formulate them as follows:

1) **Semantic Consistency.** The class definitions of datasets are various, but they can be mapped to our semantic space with the fewest semantic damages. The mapping is completed via crowd-sourced annotation with the help of word embedding distances. Only *one-time alignment* is required for a dataset. As more and more classes are aligned and covered, the process would be faster and faster with synonyms checking. As shown in Fig. 1, our semantic space covers a broad range of semantics, verifying this mapping.

2) **Temporal Consistency.** Some videos [4] only have sparse labels for a whole clip instead of each frame. We sample the clip with  $3\text{fps}$  and give frames the label of their belonged clip. We provide both frame- and clip-level labels.

3) **Spatial Consistency.** There are both instance (boxes) [27] and image [8] level labels. We merge the instance labels of each image/frame into image/frame-level labels. For demands of instance-level training, we can still use the original instance-level labels [20, 27] and detectors [71, 54] to get instance boxes for future annotation.

4) **3D Format Consistency.** 3D datasets typically have various formats, e.g., SMPL [70] has 24 keypoints while CMU MoCap [6] has 31 keypoints. To keep consistency, we transform all of them into SMPL via a fitting procedure.

5) **2D-3D Consistency.** Image/video datasets mostly contain only 2D labels without GT 3D humans. Aside from the GT 3D humans from 3D datasets [25], we recover 3D humans from 2D data as *pseudo* 3D labels via ROMP [72] and EFT [73]. We use both GT and pseudo 3D humans in 3D action recognition and generation. Though the reconstruction is sometimes noisy, we use the pseudo 3D humans as a noisy data augmentation to supplement 2D learning. In tests, we find that 2D and 3D learning are complementary.

**Analysis.** With the large data collection and unified se-

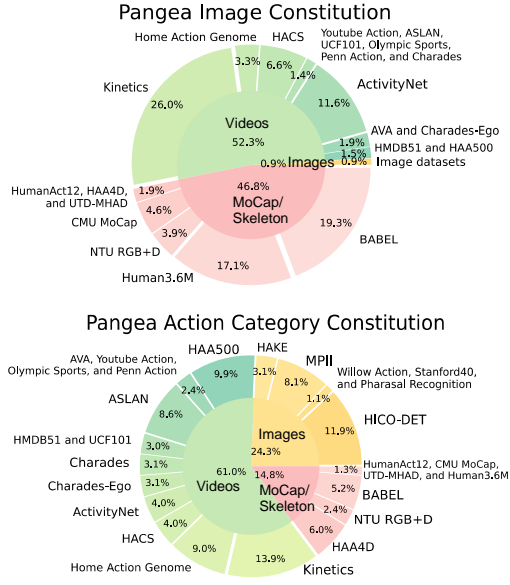


Figure 3: Gathered datasets in *Pangea*.

semantic space, we build *Pangea* as shown in Fig. 3. It contains **10.9 M** images, **1.2 M** videos, and **110 K** 3D humans over **28** datasets, with coverage of **4 K+** action classes of original datasets. About 27.7% of Kinetics-400 [10] data is covered for training efficiency. *Pangea* covers the semantics of **513** verb nodes over all the 898 nodes of VerbNet [13] and includes **290** leave nodes carrying fine-grained semantics. Its train set has 10.7 M images and the test set has 178 K images. To evaluate few/zero-shot learning, we split the 290 leave nodes into two sets and evaluate them separately: *rare* (133 leave nodes) and *non-rare* (157 leave nodes).

## 5. Methodology

### 5.1. Physical-to-Semantic Space Mapping

We first introduce the Physical-to-Semantic Space (P2S) mapping (Fig. 4). We aim to propose a multi-modal, concise, and practical model as the baseline and inspire future work. Given a sample of the physical space  $P$ , we obtain its representation  $V$  via different encoders according to its modality. For images, we use a CNN/Transformer-based image encoder. For videos, we first input them to the image encoder for frame encoding then use a temporal layer for temporal encoding. For SMPLs, we convert them into point clouds and use a PointNet++[74] as the encoder that performs best in our test (detailed in the supplementary).

In the semantic space  $S$ , we define  $N$  target verb nodes. For each node, two types of information are provided by VerbNet [13]: 1) **semantic** one to describe its meaning, *e.g.*, example sentences, WordNet definitions; 2) **geometry** one to locate it in the hierarchical tree and reveal its connection with the other nodes. They are encoded into *representation*  $T = \{t_i\}_{i=1}^N$  and  $G = \{g_i\}_{i=1}^N$  via a text encoder and geometry encoder respectively. The ground-truth (GT) label

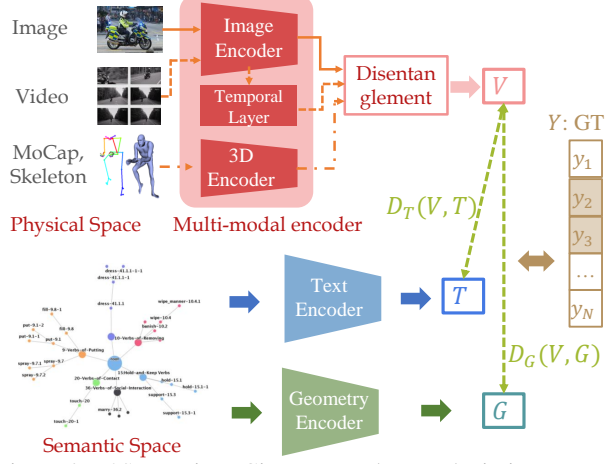


Figure 4: P2S mapping. Given a sample, we obtain its representation  $V$  via different encoders.  $V$  is then aligned with semantic and geometry representations  $T$  and  $G$  under the supervision of  $Y$ .  $V_{raw}$  to  $V$  is omitted for clarity.

for the sample is  $Y = \{y_i | y_i \in \{0, 1\}\}_{i=1}^N$ . P2S mapping is a *multi-label* classification, where a physical sample is mapped to multi-node of the semantic space (**one-to-many** mapping). Thus, we have the loss function as:

$$\mathcal{L}_{node} = \mathcal{L}_{cls}(\mathcal{D}_T(V, T), Y) + \alpha \cdot \mathcal{L}_{cls}(\mathcal{D}_G(V, G), Y), \quad (1)$$

where  $\mathcal{D}_T(\cdot, \cdot)$  and  $\mathcal{D}_G(\cdot, \cdot)$  measure the distances between  $V$  and  $T, G$  respectively,  $\mathcal{L}_{cls}$  is a Binary Cross Entropy loss for multi-label classification and  $\alpha$  balances the loss weight.

#### 5.1.1 Semantic Disentanglement and Augmentation

A person typically performs multi-action simultaneously, *e.g.*, standing while eating. Such **entanglement** of multi-action semantics increases the annotation and learning difficulty. It is a challenge to annotate all the ongoing actions of a person in previous datasets since the *limited coverage* and *ambiguity* of their classes. Besides, as *Pangea* has a broader semantic space, after the *action*  $\rightarrow$  *node* mapping in Sec. 4, we face a **partly-labeling** problem. Moreover, in the mapping, some labels are early filtered out without labels, and a few of them should have been annotated as True. Also, errors of omission may still exist within the labels because of annotators' varied understanding. Thus, each sample theoretically has a partial annotation  $Y = \{y_i | y_i = 1, 0, \emptyset\}_{i=1}^N$ , where 1, 0 are certain positive/negative labels, and  $\emptyset$  is *uncertain*. Though it is nearly impossible to supplement the labels of all  $N$  verb nodes in *Pangea* for all 20 M samples (images/videos/MoCap), we can conduct flexible *weakly-supervised* learning with partly-labeled data with representation disentanglement.

To facilitate the one-to-many P2S mapping and address the partly-labeling problem, we propose to disentangle a physical representation into **node-specific** representations. Here, we use  $V_{raw}$  as the entangled physical feature.

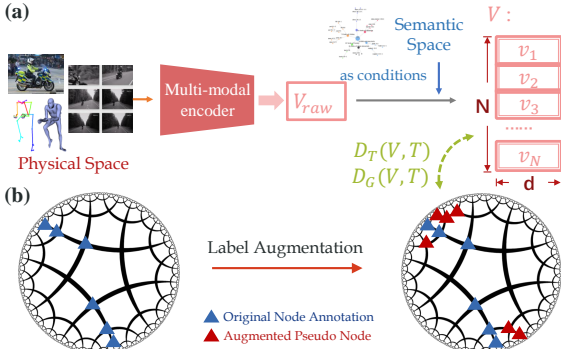


Figure 5: Semantic disentangle and augmentation. (a) The entangled physical representation  $V_{\text{raw}}$  is transformed into node-specific representation  $V = \{v_i\}_{i=1}^N \in \mathbf{R}^{N \times d}$  ( $i$ : node index) as *conditions*. (b) Generating pseudo node labels via language priors and structure knowledge.

Thanks to our *unambiguous* verb node definition, we can disentangle the input  $V_{\text{raw}}$  into  $N$  representations supervised by  $N$  verb nodes respectively. Thus, the gradients of verb nodes (True/False labeled clearly) can be disentangled during training from the uncertain ones.

As is illustrated in Fig. 5, a model is trained to transform the entangled physical representation  $V_{\text{raw}} \in \mathbf{R}^d$  ( $d$ : dimension) into node-specific representation  $V = \{v_i\}_{i=1}^N \in \mathbf{R}^{N \times d}$  ( $i$ : verb node index) as conditions. In detail, we first define the verb node-specific disentangling mapping function  $f_i$  for the  $i$ -th node, which is in practice a learnable MLP. Then, given  $V_{\text{raw}}$ ,  $f_i(\cdot)$  transforms it into  $v_i = f_i(V_{\text{raw}})$ . Finally, each  $v_i$  would be used for semantic alignment via  $\mathcal{D}_T(v_i, t_i) = \text{Sigmoid}(\gamma \cdot \cos(v_i, t_i))$ , where  $\cos(\cdot, \cdot)$  is the cosine similarity and  $\gamma$  is a scaling factor. If not disentangled, it goes like  $\mathcal{D}_T(V_{\text{raw}}, t_i) = \text{Sigmoid}(\gamma \cdot \cos(V_{\text{raw}}, t_i))$ , *i.e.*, physical representation for classification is shared by all verb nodes.

Aside from disentanglement, the partly-labeling problem can also be alleviated by augmenting the GT label  $Y$ . As the verb nodes in our structure semantic space have clear semantic and geometric relations in a tree, we propose a label augmentation method to generate pseudo node labels for missing ones via language priors and structure knowledge. For more details, please refer to the supplementary.

### 5.1.2 Verb Node Semantic Encoding and Alignment

Next, we discuss how to use text representation to encode semantic information of nodes into  $T = \{t_i\}_{i=1}^N \in \mathbf{R}^{N \times d}$  and calculate  $\mathcal{D}_T(V, T)$ . As mentioned in Sec. 3, the node semantic information includes: 1) verb members; 2) example sentences; 3) WordNet [14] definition and FrameNet [16] mapping for each verb member. Following CLIP [11],  $T$  is obtained via inputting the above text descriptions into a Transformer encoder. Then, for the *labeled*  $i$ -th node, we have  $\mathcal{D}_T(v_i, t_i) = \text{Sigmoid}(\gamma \cdot \cos(v_i, t_i))$ .

Different from CLIP [11] where the text is short (up to 77 tokenized symbols, or equally 30 words approximately), our node description is much longer (up to 2 K words). It is inefficient and memory-costly to directly input such long text into the encoder. Thus, we propose two efficient ways below.

**Text Sampling.** For a node, we have  $n$  sentences  $\{sent_i\}_{i=1}^n$  to describe it and each sentence  $sent_i$  is composed of  $n_i$  words, *i.e.*,  $sent_i = \{word_{ij}\}_{j=1}^{n_i}$ . We have  $\sum_i n_i$  words as candidates. We sample key texts clarifying the node semantics better. We use TextRank [75] to extract keywords  $word_{ij}$  from  $\{sent_i\}_{i=1}^n$ . Then we take the **summarized** text as the text encoder input.

**Pretrained Language Vectors.** Besides sampling, we alternatively compress the texts and encode all of them. Each  $sent_i = \{word_{ij}\}_{j=1}^{n_i}$  is first encoded into  $l_i$  via a pretrained text encoder [11]. Then for  $\{sent_i\}_{i=1}^n$ , we get  $\{l_i\}_{i=1}^n$ , which is fed into the text encoder as tokens.

A performance comparison of them is given in the supplementary, two strategies perform comparably. The possible reason is that there may be a trade-off exists between the encoded text length and learning difficulty. However, given a more powerful large language model [17] to fully utilize the diverse semantic information of verb nodes, things may be different. We leave this to future work.

### 5.1.3 Verb Node Geometry Encoding and Alignment

Next, we discuss how to encode the geometry information into  $G = \{g_i\}_{i=1}^N \in \mathbf{R}^{N \times d}$  and calculate  $\mathcal{D}_G(V, G)$  (Fig. 6). To encode the hierarchy, parent-child relation, verb tree depth, *etc.*, we construct a continuous Poincaré ball to embed the discrete verb tree. Besides, to utilize the representative ability of language models [76, 11], we also propose a geometric prompt strategy to strengthen the training.

**Poincaré Action Semantic Space.** To encode the node positions, we embed them into *hyperbolic* space, a  $n$ -dimensional Poincaré ball. Hyperbolic space can be thought of as a continuous version of a tree and as such, it is naturally equipped to model hierarchical structures, where original node distances are preserved approximately. Given the hierarchy defined in VerbNet [13], we obtain hyperbolic embeddings for nodes with Riemannian optimizer following the setting of [77]. Since there are only 898 nodes, they can be encoded into a low-dimensional Poincaré ball [77]. In practice, we set the dimension  $n = 2$ . The learned hyperbolic embeddings for all verb nodes are visualized in Fig. 6. More details about the Poincaré ball construction and optimization are provided in the supplementary.

With the hyperbolic embeddings  $G$ , we measure  $\mathcal{D}_G(V, G)$  and align  $V$  with  $G$ . Huge dimension gap exists between  $V = \{v_i\}_{i=1}^N$  and  $G = \{g_i\}_{i=1}^N$ :  $g_i$  is 2-d while  $v_i$  is of much higher dimension. Intuitively, we can

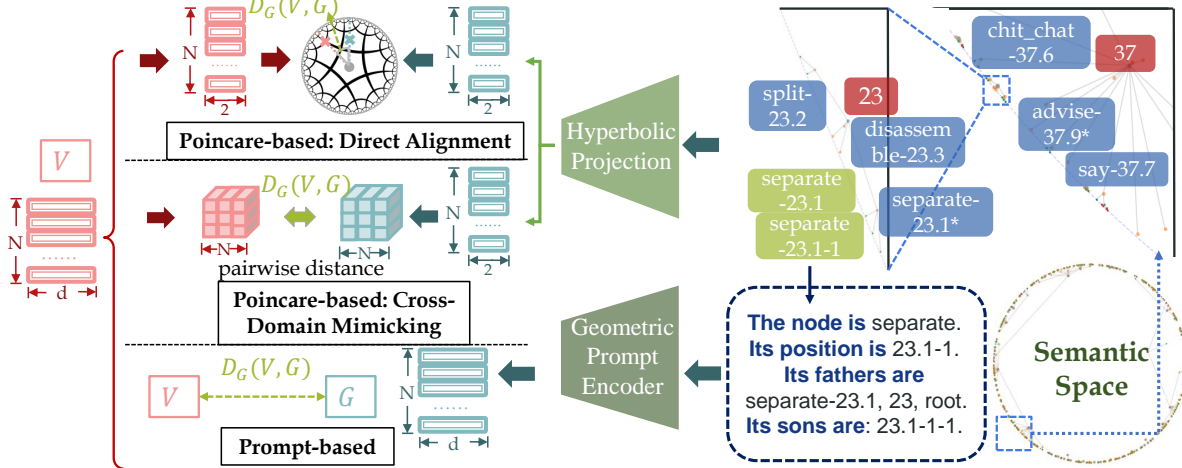


Figure 6: Geometry information encoding and P2S mapping ( $V$  to  $G$ ). 1) The *right* part: the learned Poincaré ball embedding the verb tree (Right→left: coarse→fine level; Red, blue, green: high→low level). 2) The *left* part: different geometry alignment methods.

map  $v_i$  to the Poincaré ball and **directly align** them in the hyperbolic space. However, an obvious weakness is the information loss of  $V$ . Intuitively raising the dimension of  $G$  also degrades performance in our tests. A possible reason is that a higher dimensional Poincaré ball embedding only 898 nodes is too *sparse* thus hindering the training.

Thus, we propose a more simple method: **cross-domain mimicking**, where  $\mathcal{D}_G(V, G)$  is measured without compressing  $V$ . Instead of measuring the distance between  $v_i$  and  $g_i$  directly, we encourage the two domains to share similar inner structures, *i.e.*, enforce  $V$  mimicking the change of  $G$ . First, we compute *pairwise distance matrix* of  $G$  as  $M_G = (d_{i,j}) \in \mathbf{R}^{N \times N}$ . Then, the distance indicator  $\Gamma \in \{-1, 0, 1\}^{N \times N \times N}$  is generated via

$$\Gamma_{i,j,k} = \begin{cases} -1, & \text{if } d_{j,i} < d_{k,i}, \\ 0, & \text{if } d_{j,i} = d_{k,i}, \\ 1, & \text{if } d_{j,i} > d_{k,i}, \end{cases} \quad (2)$$

where  $\Gamma_{i,j,k}$  demonstrates the relative distance relation between nodes  $j, k$  with respect to the reference node  $i$ . Meanwhile, the *pairwise distance matrix* of  $V$  is  $M_V = (d'_{i,j}) \in \mathbf{R}^{N \times N}$  and the indicator is  $\Gamma' \in \mathbf{R}^{N \times N \times N}$ , where  $\Gamma'_{i,j,k} = d'_{j,i} - d'_{k,i}$ . Thus, we devise the mimicking loss as

$$\mathcal{L}_{mim} = \sum_{j,k} \max(-\Gamma_{i,j,k} \hat{\Gamma}_{i,j,k}, 0). \quad (3)$$

For a sample,  $\mathcal{L}_{mim}$  is only computed for the *labeled* node  $i$ . If a sample reflects the semantics of the  $i$ -th node, its disentangled  $v_i$  should have similar pairwise distance relation. Specifically, if node  $i$  is closer to  $j$  than  $k$ , then  $v_i$  should behave similarly,  $v_i$  is closer to  $v_j$  than  $v_k$ . With this regulation, we can align the two spaces without compression.

**Geometric Prompt.** Alternatively, the geometry information can also be described via natural language as

Method	Full	Rare	Non-Rare
CLIP	28.25	16.90	37.87
P2S	34.36	21.75	45.05
P2S-aug	<b>34.46</b>	<b>21.84</b>	<b>45.15</b>

Table 1: Verb node classification results on *Pangea* test set.

prompts, *e.g.*, the node “touch-20-1” is described as: “The node is touch. Its position is 20-1. Its ancestors are touch-20, 20, and root. Its descendants are none.” Then, we use a text encoder to encode these texts. Thus,  $G$  and  $\mathcal{D}_G(V, G)$  is obtained in a similar way as  $T$  and  $\mathcal{D}_T(V, T)$ . When using hyperbolic embeddings to encode  $G$ , we can adopt Eq. 1 to calculate the loss. However, for geometric prompt, it is costly to directly combine  $\mathcal{D}_T(V, T)$  and  $\mathcal{D}_G(V, G)$  with two text encoders for  $T$  and  $G$ . To address this, we propose some efficient ways to combine  $\mathcal{D}_T(V, T)$  and  $\mathcal{D}_G(V, G)$ :

1) **Text concatenation.** We concatenate the sentences of semantic and geometric information and input them together into one text encoder and get representation  $TG$ . Here,  $T$  and  $G$  are combined implicitly in the model.

2) **Prediction Fusion.** Two models are trained to align  $V \& T$  and  $V \& G$  respectively. The unified distance  $\mathcal{D}_{TG}(V, TG)$  is fused via  $\beta_T \cdot \mathcal{D}_T(V, T) + \beta_G \cdot \mathcal{D}_G(V, G)$ , where  $\beta_T$  and  $\beta_G$  are learnable weights.

3) **Training Alternately.** We alternately train  $\mathcal{D}_T(V, T)$  and  $\mathcal{D}_G(V, G)$  with one text encoder, *e.g.*, the first epoch for one and the next epoch for the other.

#### 5.1.4 Training and Inference

In training, our semantic encoding can involve the original action labels of samples too. In most cases, this helps but is more memory-costly. If adopting the original labels as a supplement, we have a loss  $\mathcal{L}_{ori}$  to align the physical feature with the text feature of the original labels. The total loss is then  $\mathcal{L}_{P2S} = \mathcal{L}_{ori} + \mathcal{L}_{node}$ . In inference, P2S output probabilities of both original action classes  $\mathcal{S}_{ori}$  and verb

Method	mAP
R*CNN [78]	28.5
Mallya <i>et al.</i> [79]	36.1
Pairwise [80]	39.9
ReLVIT [81]	40.1
CLIP [11]	46.1
CLIP-Pangea	47.4
P2S	<b>48.5</b>

Table 2: Results on the image benchmark HICO [8].

Method	Top-1 Accuracy (%)
I3D [82]	33.53
TPN [83]	50.53
TSN [84]	55.33
EVL [85]	76.40
CLIP [11]	63.33
CLIP [11]-Pangea	67.20
P2S	68.73
P2S + EVL [85]	<b>79.80</b>

Table 3: Results on the video benchmark HAA [9].

Method	Top-1 Accuracy (%)
TSN [84]	69.40
RGB-I3D [82]	74.30
Two-stream I3D [82]	80.90
EVL [85]	83.60
CLIP [11]	63.49
CLIP [11]-Pangea	64.48
P2S	65.99
P2S + EVL [85]	<b>87.46</b>

Table 4: Results on the video benchmark HMDB51 [57].

Method	mAP (%)
I3D [82]	32.90
MViT-B-24 [86]	47.70
DEEP-HAL w/ ODF+SDF [87]	50.16
MoViNet-A5 [88]	53.19
CLIP [11]	39.71
CLIP [11]-Pangea	42.59
P2S	45.81
P2S + MoViNet-A5 [88]	<b>60.55</b>

Table 5: Results on the video benchmark Charades [89].

Table 6: Results on the video benchmark Kinetics-400 [10].

Table 7: Results on the 3D benchmark BABEL-120 [25].

nodes  $\mathcal{S}_{node}$ . We evaluate node classification with  $\mathcal{S}_{node}$  on *Pangea*. For transfer learning, we evaluate multi-label classification on downstream benchmarks with  $\mathcal{S}_{ori}$  and  $\mathcal{S}_{node}$ . We use a small learnable MLP to transform  $\mathcal{S}_{node}$  to  $\mathcal{S}'_{ori}$  and obtain the final output via fusing  $\mathcal{S}_{ori}$  and  $\mathcal{S}'_{ori}$ .

## 5.2. Semantic-to-Physical Space Mapping

Though we focus on P2S mapping, with the learned abundant semantic representation of nodes and the collected 3D data, we wonder if we can do the inverse mapping, *i.e.*, Semantic-to-Physical space (S2P). S2P should be scalable to different semantic granularities and flexible with either **single**- or **multi**-node and generate reasonable 3D motions. We propose a simple model to verify our assumption. We train a cVAE conditioned on the node semantic and geometric features  $T, G$  to map  $S$  to  $P$ . The encoder takes  $T, G$  and  $V$  as input, outputting the mean  $\mu$  and log-variance  $\sigma$  for a Gaussian distribution, from which we sample a latent encoding  $z$ .  $z$  is concatenated with  $T, G$  then fed to the decoder, getting the reconstructed  $V'$ . We adopted SMPL [70] parameters as  $V$ . For a sample belonging to multiple nodes, we take the mean of its corresponding  $T, G$  as the condition. We train S2P on the 3D data of *Pangea*, using KL divergence driving the predicted distribution to normal distribution and an L2 reconstruction loss of the SMPL parameters.

## 6. Experiment

### 6.1. Dataset and Implementation

**Dataset.** *Pangea* is a multi-modal benchmark to evaluate node classification. We also conduct transfer learning on widely-used multi-modal benchmarks: HICO [8], HAA [9], Charades [89], HMDB51 [57], Kinetics-400 [10], BABEL [25], and HAA4D [91].

**Implementation.** (1) P2S training: we use 10.7 M 2D images/frames and 840 K 3D humans. (2) P2S transfer learning: P2S pretrained on *Pangea* with node classification is a knowledgeable **backbone**. To make the transfer

Table 8: Results on the 3D benchmark HAA4D [91].

Table 9: Ablation studies on the proposed benchmark *Pangea*.

learning strict, in pretraining, we **exclude** the train & test set data of the downstream dataset from *Pangea* train set. Then the pre-trained backbone is finetuned and tested on downstream datasets. For different modalities, we use their corresponding data path. To make our pipeline efficient, we do not adopt complex temporal encoding and video augmentation. Instead, we use *simple* strategies to implement the temporal encoding similar to [92], *e.g.*, mean pooling, a temporal transformer, average prediction of frames, *etc*. P2S is a multi-modal and lite pipeline that is different from the ad-hoc models for sole-modal tasks. We can use it as a **plug-and-play**, *i.e.*, fusing it with SOTA models in downstream tasks. Moreover, as P2S is trained in much broader semantic coverage on large-scale data, its learned bias is different from ad-hoc models. Thus, P2S is complementary to these SOTA models and can further improve their performances. Besides, we test different ways to fuse 2D and 3D to mine the potential of multi-modal learning. The simplest *late fusion* (fusing logits) performs best in our tests. Thus, we use late fusion as the default. For data with one human per image/frame, we fuse the 2D and 3D results. While for data with more than one human per image/frame, we first conduct *max pooling* on the 3D results of multi-human then perform late fusion with 2D. (3) S2P training: the text and geometry encoders of P2S are used to encode the information as conditions and *frozen*. All experiments are conducted on **four** NVIDIA RTX 3090 GPUs.

### 6.2. Action Recognition and Generation

**Verb Node Classification on *Pangea*.** We report the results in Tab. 1. For baseline *CLIP*, we load the vanilla *CLIP* pre-trained model [11] as the backbone and train it on *Pangea* train set for node classification. We use visual-language alignment in training and use the same texts as P2S in inference. It achieves 28.25 mAP on 290 leave nodes (16.90 mAP for 133 rare nodes, 37.87 mAP for 157 non-rare nodes). Relatively, P2S performs much better with the help of disentanglement and semantic/geometric alignment. It achieves **34.36** mAP (**21.75** for rare nodes, and **45.05** for

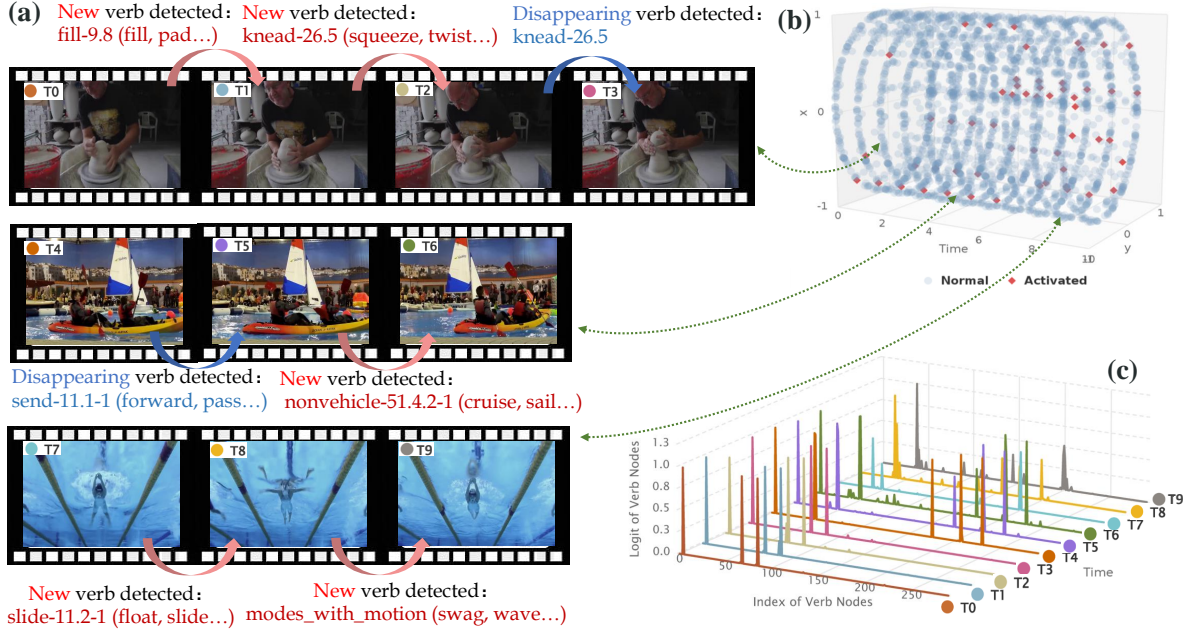


Figure 7: Continuous semantic change. We show the results of 3 videos from *Pangea* test set. a) Frames and analysis of the changed node predictions. b) Visualization of predictions of all verb nodes in the Poincaré ball (red: verb nodes with high probabilities). c) Detailed predictions of all verb nodes (peak: verb nodes with high probabilities).

non-rare nodes). Moreover, with label augmentation, P2S-aug further outperforms P2S on all three tracks.

**Transfer Learning.** We refer to the downstream benchmark as the *target*. For a fair comparison, we design several baselines: (1) *CLIP*: finetuning the vanilla CLIP pre-trained model on target train set and testing it on target test set; (2) *CLIP-Pangea*: finetuning the vanilla CLIP pre-trained model on *Pangea* train set with  $\mathcal{L}_{ori}$ , then finetuning it on target train set, where  $\mathcal{S}_{ori}$  is used for evaluation on target test set.

**Image Benchmark.** In Tab. 2, *CLIP* performs well and even outperforms the ad-hoc SOTA models on HICO [8]. Given the image-text pairs from *Pangea*, *CLIP-Pangea* outperforms *CLIP* with 1.3 mAP. However, *CLIP-Pangea* cannot utilize the extensive semantic-geometric knowledge. Thus, P2S boosts the performance and outperforms RelViT and *CLIP* with **8.4** and **2.4** mAP respectively.

**Video Benchmark.** The *CLIP*, *CLIP-Pangea* are with the same setting as above. The conclusion is similar in Tab. 3-6. *CLIP-Pangea* weaponized with *Pangea* outperforms *CLIP*. And P2S outperforms *CLIP* with **5.40%**, **2.50%**, **6.10%**, and **1.93%** respectively. Moreover, P2S without bells and whistles performs comparable (e.g., TSN on HMDB51, MViT-B-24 on Charades, TSN on Kinetics-400) or even better (e.g., TSN on HAA) than SOTA video models. Lastly, fusing P2S and SOTA models further improves the performances: **3.40%** (HAA), **3.86%** (HMDB51), **7.36** mAP (Charades), and **1.41%** (Kinetics-400).

**3D Recognition.** We set two baselines *PointNet++* and *CLIP* and strengthen them with *Pangea* as *PointNet++-Pangea*.

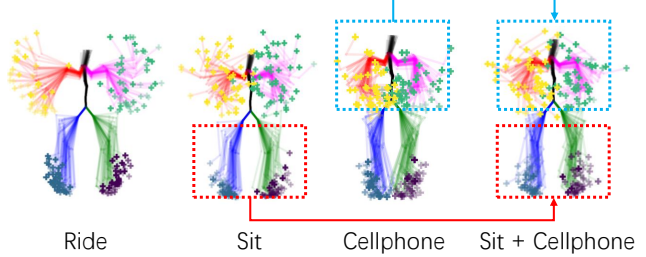


Figure 8: S2P results. *ride* has the elbows away from the spine, while *sit* has the opposite. Adding *cellphone* upon *sit* drives the wrist to distribute around the pelvis more.

**Pangea and CLIP-Pangea.** Similarly, *PointNet++-Pangea* and *CLIP-Pangea* performs better in Tab. 7, 8. And P2S outperforms all the baselines, e.g. **7.43%** upon *PointNet++* on BABEL. Moreover, P2S performs better than the ad-hoc SOTA thanks to the abundant training data of *Pangea*. We do not fuse P2S with SOTA here due to the modality gap: most SOTA use 3D skeleton while we use point cloud.

**Visualization.** We analyze the ability of P2S to detect continuous semantic changes in videos in Fig. 7. Besides, we report the result of S2P (Sec. 5.2) in Fig. 8, verifying that S2P is capable of generating reasonable poses for single/multi-node. For more results, limitations, and discussions, please refer to the supplementary.

**Ablation Study & Discussion.** We conduct ablations on *Pangea* to evaluate the P2S components in Tab. 9 and supplementary. Without 3 key components, P2S shows obvious degradation, which follows the gap between P2S and *CLIP-Pangea*. Moreover, semantic disentanglement matters most to facilitate the one-to-many P2S mapping and

weakly-supervised learning. In this work, we adopt concise models to verify the efficacy of *Pangea* and quickly trial-an-error with limited GPUs. We believe that larger and more sophisticated models trained with *Pangea* with more computing power would gain more superiority in future work.

## 7. Conclusion

In this work, to bridge the “isolated islands” in action understanding, we propose a structured action semantic space and accordingly merge multi-modal datasets into a unified *Pangea* benchmark. Moreover, to fully use *Pangea*, we propose a bidirectional mapping system to afford action recognition and 3D action generation showing superiority. We believe our framework paves a new path for future study.

## References

[1] Helen L Egger, Geraldine Dawson, Jordan Hashemi, Kimberly LH Carpenter, Steven Espinosa, Kathleen Campbell, Samuel Brotkin, Jana Schaich-Borg, Qiang Qiu, Mariano Tepper, et al. Automatic emotion and attention analysis of young children at home: a researchkit autism feasibility study. *NPJ digital medicine*, 2018. 1

[2] Laura Smith, Nikita Dhawan, Marvin Zhang, Pieter Abbeel, and Sergey Levine. Avid: Learning multi-stage tasks via pixel-level translation of human videos. *arXiv preprint arXiv:1912.04443*, 2019. 1

[3] Yong-Lu Li, Xinpeng Liu, Xiaoqian Wu, Yizhuo Li, Zuoyu Qiu, Liang Xu, Yue Xu, Hao-Shu Fang, and Cewu Lu. Hake: A knowledge engine foundation for human activity understanding. *TPAMI*, 2023. 1, 2, 28

[4] Joao Carreira, Eric Noland, Chloe Hillier, and Andrew Zisserman. A short note on the kinetics-700 human action dataset. *arXiv preprint arXiv:1907.06987*, 2019. 1, 2, 3, 14, 16, 20

[5] Catalin Ionescu, Dragos Papava, Vlad Olaru, and Cristian Sminchisescu. Human3. 6m: Large scale datasets and predictive methods for 3d human sensing in natural environments. *TPAMI*, 2013. 1, 2, 16

[6] Chuan Guo, Xinxin Zuo, Sen Wang, Shihao Zou, Qingyao Sun, Annan Deng, Minglun Gong, and Li Cheng. Action2motion: Conditioned generation of 3d human motions. In *ACMMM*, 2020. 1, 2, 3, 15, 16, 20

[7] Amir Shahroudy, Jun Liu, Tian-Tsong Ng, and Gang Wang. Ntu rgb+ d: A large scale dataset for 3d human activity analysis. In *CVPR*, 2016. 1, 16

[8] Yu Wei Chao, Zhan Wang, Yugeng He, Jiaxuan Wang, and Jia Deng. Hico: A benchmark for recognizing human-object interactions in images. In *ICCV*, 2015. 1, 2, 3, 7, 8, 14, 16, 18, 21

[9] Jihoon Chung, Cheng hsin Wuu, Hsuan ru Yang, Yu-Wing Tai, and Chi-Keung Tang. Haa500: Human-centric atomic action dataset with curated videos. In *ICCV*, 2021. 1, 7, 16, 18, 20, 21

[10] Will Kay, Joao Carreira, Karen Simonyan, Brian Zhang, Chloe Hillier, Sudheendra Vijayanarasimhan, Fabio Viola, Tim Green, Trevor Back, Paul Natsev, et al. The kinetics human action video dataset. *arXiv preprint arXiv:1705.06950*, 2017. 1, 2, 4, 7, 19, 21, 22

[11] Alec Radford, Jong Wook Kim, Chris Hallacy, Aditya Ramesh, Gabriel Goh, Sandhini Agarwal, Girish Sastry, Amanda Askell, Pamela Mishkin, Jack Clark, et al. Learning transferable visual models from natural language supervision. In *ICML*, 2021. 1, 2, 3, 5, 7, 14, 27, 28

[12] Tianyu Gao, Xingcheng Yao, and Danqi Chen. SimCSE: Simple contrastive learning of sentence embeddings. In *EMNLP*, 2021. 2, 15, 17

[13] Karin Kipper Schuler. *VerbNet: A broad-coverage, comprehensive verb lexicon*. University of Pennsylvania, 2005. 2, 3, 4, 5, 23

[14] George A Miller. Wordnet: a lexical database for english. *Communications of the ACM*, 1995. 2, 3, 5

[15] Paul R Kingsbury and Martha Palmer. From treebank to propbank. In *LREC*, pages 1989–1993, 2002. 2

[16] Collin F Baker, Charles J Fillmore, and John B Lowe. The berkeley framenet project. In *COLING*, 1998. 2, 3, 5

[17] Tom Brown, Benjamin Mann, Nick Ryder, Melanie Subbiah, Jared D Kaplan, Prafulla Dhariwal, Arvind Neelakantan, Pranav Shyam, Girish Sastry, Amanda Askell, et al. Language models are few-shot learners. *NeurIPS*, 2020. 2, 5, 23

[18] Saurabh Gupta and Jitendra Malik. Visual semantic role labeling. *arXiv preprint arXiv:1505.04474*, 2015. 2, 16

[19] Bangpeng Yao, Xiaoye Jiang, Aditya Khosla, Andy Lai Lin, Leonidas Guibas, and Li Fei-Fei. Human action recognition by learning bases of action attributes and parts. In *ICCV*, 2011. 2

[20] Chunhui Gu, Chen Sun, David A Ross, Carl Vondrick, Caroline Pantofaru, Yeqing Li, Sudheendra Vijayanarasimhan, George Toderici, Susanna Ricco, Rahul Sukthankar, et al. Ava: A video dataset of spatio-temporally localized atomic visual actions. In *CVPR*, 2018. 2, 3, 14, 16

[21] Khurram Soomro, Amir Roshan Zamir, and Mubarak Shah. Ucf101: A dataset of 101 human actions classes from videos in the wild. *arXiv preprint arXiv:1212.0402*, 2012. 2

[22] Bernard Ghanem, Fabian Caba Heilbron, Victor Escorcia and Juan Carlos Niebles. Activitynet: A large-scale video benchmark for human activity understanding. In *CVPR*, 2015. 2, 3, 16

[23] Yong-Lu Li, Hongwei Fan, Zuoyu Qiu, Yiming Dou, Liang Xu, Hao-Shu Fang, Peiyang Guo, Haisheng Su, Dongliang Wang, Wei Wu, and Cewu Lu. Discovering a variety of objects in spatio-temporal human-object interactions. *arXiv preprint arXiv:2211.07501*, 2022. 2

[24] Jun Liu, Amir Shahroudy, Mauricio Perez, Gang Wang, Ling-Yu Duan, and Alex C Kot. Ntu rgb+ d 120: A large-scale benchmark for 3d human activity understanding. *TPAMI*, 2019. 2

[25] Abhinanda R. Punnakkal, Arjun Chandrasekaran, Nikos Athanasiou, Alejandra Quiros-Ramirez, and Michael J. Black. BABEL: Bodies, action and behavior with english labels. In *CVPR*, 2021. 2, 3, 7, 16, 19, 20, 22

[26] Yong-Lu Li, Xinpeng Liu, Xiaoqian Wu, Yizhuo Li, and Cewu Lu. Hoi analysis: Integrating and decomposing human-object interaction. In *NeurIPS*, 2020. 2

[27] Yu-Wei Chao, Yunfan Liu, Xieyang Liu, Huayi Zeng, and Jia Deng. Learning to detect human-object interactions. In *WACV*, 2018. 2, 3, 14

[28] Hao-Shu Fang, Yichen Xie, Dian Shao, Yong-Lu Li, and Cewu Lu. Decaug: Augmenting hoi detection via decomposition. In *AAAI*, 2021. 2

[29] Xinpeng Liu, Yong-Lu Li, Xiaoqian Wu, Yu-Wing Tai, Cewu Lu, and Chi-Keung Tang. Interactiveness field in human-object interactions. In *CVPR*, 2022. 2

[30] Xiaoqian Wu, Yong-Lu Li, Xinpeng Liu, Junyi Zhang, Yuzhe Wu, and Cewu Lu. Mining cross-person cues for body-part interactiveness learning in hoi detection. In *ECCV*, 2022. 2

[31] Xinpeng Liu, Yong-Lu Li, and Cewu Lu. Highlighting object category immunity for the generalization of human-object interaction detection. In *AAAI*, 2022. 2

[32] Shizhe Chen and Dong Huang. Elaborative rehearsal for zero-shot action recognition. In *ICCV*, 2021. 2

[33] Cewu Lu, Hao Su, Yonglu Li, Yongyi Lu, Li Yi, Chi-Keung Tang, and Leonidas J Guibas. Beyond holistic object recognition: Enriching image understanding with part states. In *CVPR*, 2018. 2

[34] Yong-Lu Li, Liang Xu, Xinpeng Liu, Xijie Huang, Yue Xu, Shiyi Wang, Hao-Shu Fang, Ze Ma, Mingyang Chen, and Cewu Lu. Pastanet: Toward human activity knowledge engine. In *CVPR*, 2020. 2, 16, 20, 28

[35] Yong-Lu Li, Liang Xu, Xinpeng Liu, Xijie Huang, Yue Xu, Mingyang Chen, Ze Ma, Shiyi Wang, Hao-Shu Fang, and Cewu Lu. Hake: Human activity knowledge engine. *arXiv preprint arXiv:1904.06539*, 2019. 2

[36] Yong-Lu Li, Xinpeng Liu, Han Lu, Shiyi Wang, Junqi Liu, Jiefeng Li, and Cewu Lu. Detailed 2d-3d joint representation for human-object interaction. In *CVPR*, 2020. 2

[37] Yong-Lu Li, Siyuan Zhou, Xijie Huang, Liang Xu, Ze Ma, Hao-Shu Fang, Yanfeng Wang, and Cewu Lu. Transferable interactiveness knowledge for human-object interaction detection. In *CVPR*, 2019. 2

[38] Yong-Lu Li, Xinpeng Liu, Xiaoqian Wu, Xijie Huang, Liang Xu, and Cewu Lu. Transferable interactiveness knowledge for human-object interaction detection. In *TPAMI*, 2022. 2

[39] Ankan Bansal, Sai Saketh Rambhatla, Abhinav Shrivastava, and Rama Chellappa. Detecting human-object interactions via functional generalization. *AAAI*, 2020. 2

[40] Julia Peyre, Ivan Laptev, Cordelia Schmid, and Josef Sivic. Detecting rare visual relations using analogies. In *ICCV*, 2019. 2

[41] Zhi Hou, Xiaojiang Peng, Yu Qiao, and Dacheng Tao. Visual compositional learning for human-object interaction detection. In *ECCV*, 2020. 2

[42] Joe Yue-Hei Ng, Matthew Hausknecht, Sudheendra Vijayanarasimhan, Oriol Vinyals, Rajat Monga, and George Toderici. Beyond short snippets: Deep networks for video classification. In *CVPR*, 2015. 2

[43] Jeffrey Donahue, Lisa Anne Hendricks, Sergio Guadarrama, Marcus Rohrbach, Subhashini Venugopalan, Kate Saenko, and Trevor Darrell. Long-term recurrent convolutional networks for visual recognition and description. In *CVPR*, 2015. 2

[44] Ji Lin, Chuang Gan, and Song Han. Tsm: Temporal shift module for efficient video understanding. In *ICCV*, 2019. 2

[45] Christoph Feichtenhofer, Axel Pinz, and Andrew Zisserman. Convolutional two-stream network fusion for video action recognition. In *CVPR*, 2016. 2

[46] Karen Simonyan and Andrew Zisserman. Two-stream convolutional networks for action recognition in videos. *arXiv preprint arXiv:1406.2199*, 2014. 2

[47] Christoph Feichtenhofer, Haoqi Fan, Jitendra Malik, and Kaiming He. Slowfast networks for video recognition. In *ICCV*, 2019. 2

[48] Sijie Yan, Yuanjun Xiong, and Dahua Lin. Spatial temporal graph convolutional networks for skeleton-based action recognition. In *AAAI*, 2018. 2

[49] Maosen Li, Siheng Chen, Xu Chen, Ya Zhang, Yanfeng Wang, and Qi Tian. Actional-structural graph convolutional networks for skeleton-based action recognition. In *CVPR*, 2019. 2

[50] Ziyu Liu, Hongwen Zhang, Zhenghao Chen, Zhiyong Wang, and Wanli Ouyang. Disentangling and unifying graph convolutions for skeleton-based action recognition. In *CVPR*, 2020. 2

[51] Vasileios Choutas, Philippe Weinzaepfel, Jérôme Revaud, and Cordelia Schmid. Potion: Pose motion representation for action recognition. In *CVPR*, 2018. 2

[52] An Yan, Yali Wang, Zhifeng Li, and Yu Qiao. Pa3d: Pose-action 3d machine for video recognition. In *CVPR*, 2019. 2

[53] Ashish Vaswani, Noam M. Shazeer, Niki Parmar, Jakob Uszkoreit, Llion Jones, Aidan N. Gomez, Łukasz Kaiser, and Illia Polosukhin. Attention is all you need. In *NIPS*, 2017. 2

[54] Nicolas Carion, Francisco Massa, Gabriel Synnaeve, Nicolas Usunier, Alexander Kirillov, and Sergey Zagoruyko. End-to-end object detection with transformers. In Andrea Vedaldi, Horst Bischof, Thomas Brox, and Jan-Michael Frahm, editors, *ECCV*, 2020. 2, 3

[55] Masato Tamura, Hiroki Ohashi, and Tomoaki Yoshinaga. QPIC: Query-based pairwise human-object interaction detection with image-wide contextual information. In *CVPR*, 2021. 2

[56] O. Kliper-Gross, T. Hassner, and L. Wolf. The action similarity labeling challenge. *TPAMI*, 2012. 2, 16

[57] Hildegard Kuehne, Hueihan Jhuang, Estíbaliz Garrote, Tomaso Poggio, and Thomas Serre. Hmdb: a large video database for human motion recognition. In *ICCV*, 2011. 2, 7, 16, 19, 20, 21

[58] Dian Shao, Yue Zhao, Bo Dai, and Dahua Lin. Finegym: A hierarchical video dataset for fine-grained action understanding. In *CVPR*, 2020. 2, 3

[59] Teng Long, Pascal Mettes, Heng Tao Shen, and Cees GM Snoek. Searching for actions on the hyperbole. In *CVPR*, 2020. 2, 14

[60] Spandana Gella, Mirella Lapata, and Frank Keller. Unsupervised visual sense disambiguation for verbs using multimodal embeddings. *arXiv preprint arXiv:1603.09188*, 2016. 2

[61] Tsung Yi Lin, Michael Maire, Serge Belongie, James Hays, Pietro Perona, Deva Ramanan, Piotr Dollár, and C. Lawrence Zitnick. Microsoft coco: Common objects in context. In *ECCV*, 2014. 2, 18

[62] Dieu-Thu Le, Jasper Uijlings, and Raffaella Bernardi. Tuhoi: Trento universal human object interaction dataset. In *Proceedings of the Third Workshop on Vision and Language*, 2014. 2

[63] Mathis Petrovich, Michael J. Black, and Gü̈l Varol. Action-conditioned 3D human motion synthesis with transformer VAE. In *ICCV*, 2021. 2

[64] Mathis Petrovich, Michael J. Black, and Gü̈l Varol. TEMOS: Generating diverse human motions from textual descriptions. In *ECCV*, 2022. 2

[65] Guy Tevet, Brian Gordon, Amir Hertz, Amit H Bermano, and Daniel Cohen-Or. Motionclip: Exposing human motion generation to clip space. *arXiv preprint arXiv:2203.08063*, 2022. 2

[66] Mingyuan Zhang, Zhongang Cai, Liang Pan, Fangzhou Hong, Xinying Guo, Lei Yang, and Zwei Liu. Motiondiffuse: Text-driven human motion generation with diffusion model. *arXiv preprint arXiv:2208.15001*, 2022. 2, 23

[67] Naureen Mahmood, Nima Ghorbani, Nikolaus F. Troje, Gerard Pons-Moll, and Michael J. Black. AMASS: Archive of motion capture as surface shapes. In *ICCV*, 2019. 2, 19

[68] Matthias Plappert, Christian Mandery, and Tamim Asfour. The KIT motion-language dataset. *Big Data*, 2016. 2

[69] Kaiming He, Xiangyu Zhang, Shaoqing Ren, and Jian Sun. Deep residual learning for image recognition. In *CVPR*, 2016. 3

[70] Matthew Loper, Naureen Mahmood, Javier Romero, Gerard Pons-Moll, and Michael J. Black. SMPL: A skinned multi-person linear model. *SIGGRAPH Asia*, 2015. 3, 7, 14, 15, 19, 20, 26

[71] Shaoqing Ren, Kaiming He, Ross Girshick, and Jian Sun. Faster r-cnn: Towards real-time object detection with region proposal networks. In *NIPS*, 2015. 3

[72] Yu Sun, Qian Bao, Wu Liu, Yili Fu, Black Michael J., and Tao Mei. Monocular, one-stage, regression of multiple 3d people. In *ICCV*, 2021. 3, 14, 15, 16, 20, 26, 27

[73] Hanbyul Joo, Natalia Neverova, and Andrea Vedaldi. Exemplar fine-tuning for 3d human model fitting towards in-the-wild 3d human pose estimation. *arXiv preprint*, 2020. 3, 16, 20

[74] Charles Ruizhongtai Qi, Li Yi, Hao Su, and Leonidas J Guibas. Pointnet++: Deep hierarchical feature learning on point sets in a metric space. *NIPS*, 2017. 4, 7, 19, 20, 26

[75] Paco Nathan. Pytextrank, a python implementation of textrank for phrase extraction and summarization of text documents. [Online] <https://github.com/DerwenAI/pytextrank>, 2016. 5

[76] Jacob Devlin, Ming-Wei Chang, Kenton Lee, and Kristina Toutanova. Bert: Pre-training of deep bidirectional transformers for language understanding. *arXiv preprint arXiv:1810.04805*, 2018. 5

[77] Maximillian Nickel and Douwe Kiela. Poincaré embeddings for learning hierarchical representations. *NIPS*, 2017. 5, 14, 17

[78] Georgia Gkioxari, Ross Girshick, and Jitendra Malik. Contextual action recognition with r\* cnn. In *ICCV*, 2015. 7

[79] Arun Mallya and Svetlana Lazebnik. Learning models for actions and person-object interactions with transfer to question answering. In *ECCV*, 2016. 7

[80] Hao Shu Fang, Jinkun Cao, Yu Wing Tai, and Cewu Lu. Pairwise body-part attention for recognizing human-object interactions. In *ECCV*, 2018. 7

[81] Xiaojian Ma, Weili Nie, Zhiding Yu, Huaizu Jiang, Chaowei Xiao, Yuke Zhu, Song-Chun Zhu, and Anima Anandkumar. Relvit: Concept-guided vision transformer for visual relational reasoning. *arXiv preprint arXiv:2204.11167*, 2022. 7

[82] Andrew Zisserman Joao Carreira. Quo vadis, action recognition? a new model and the kinetics dataset. In *CVPR*, 2017. 7

[83] Ceyuan Yang, Yinghao Xu, Jianping Shi, Bo Dai, and Bolei Zhou. Temporal pyramid network for action recognition. In *CVPR*, 2020. 7

[84] Limin Wang, Yuanjun Xiong, Zhe Wang, Yu Qiao, Dahua Lin, Xiaoou Tang, and Luc Van Gool. Temporal segment networks: Towards good practices for deep action recognition. In *ECCV*, 2016. 7

[85] Ziyi Lin, Shijie Geng, Renrui Zhang, Peng Gao, Gerard de Melo, Xiaogang Wang, Jifeng Dai, Yu Qiao, and Hongsheng Li. Frozen clip models are efficient video learners. *arXiv preprint arXiv:2208.03550*, 2022. 7, 14, 20, 21, 22

[86] Haoqi Fan, Bo Xiong, Karttikeya Mangalam, Yanghao Li, Zhicheng Yan, Jitendra Malik, and Christoph Feichtenhofer. Multiscale vision transformers. In *ICCV*, 2021. 7

[87] Lei Wang and Piotr Koniusz. Self-supervising action recognition by statistical moment and subspace descriptors. In *ACMMM*, 2021. 7

[88] Dan Kondratyuk, Liangzhe Yuan, Yandong Li, Li Zhang, Mingxing Tan, Matthew Brown, and Boqing Gong. Movinets: Mobile video networks for efficient video recognition. In *CVPR*, 2021. 7, 21

[89] Gunnar A Sigurdsson, Gü̈l Varol, Xiaolong Wang, Ali Farhadi, Ivan Laptev, and Abhinav Gupta. Hollywood in homes: Crowdsourcing data collection for activity understanding. In *ECCV*, 2016. 7, 16, 19, 20, 21

[90] Zhan Tong, Yibing Song, Jue Wang, and Limin Wang. Videomae: Masked autoencoders are data-efficient learners for self-supervised video pre-training. *arXiv preprint arXiv:2203.12602*, 2022. 7

[91] Mu-Ruei Tseng, Abhishek Gupta, Chi-Keung Tang, and Yu-Wing Tai. Haa4d: Few-shot human atomic action recognition via 3d spatio-temporal skeletal alignment, 2022. 7, 16, 20, 22

[92] Mengmeng Wang, Jiazheng Xing, and Yong Liu. Actionclip: A new paradigm for video action recognition. *arXiv preprint arXiv:2109.08472*, 2021. 7, 14

[93] Alexandru Tifrea, Gary Bécigneul, and Octavian-Eugen Ganea. Poincaré glove: Hyperbolic word embeddings. *arXiv preprint arXiv:1810.06546*, 2018. **14, 17**

[94] Octavian Ganea, Gary Bécigneul, and Thomas Hofmann. Hyperbolic entailment cones for learning hierarchical embeddings. In *ICML*, 2018. **14**

[95] Dídac Surís, Ruoshi Liu, and Carl Vondrick. Learning the predictability of the future. In *CVPR*, 2021. **14**

[96] Valentin Khrulkov, Leyla Mirvakhabova, Evgeniya Ustinova, Ivan Oseledets, and Victor Lempitsky. Hyperbolic image embeddings. In *CVPR*, 2020. **14**

[97] Ankit Dhall, Anastasia Makarova, Octavian Ganea, Dario Pavllo, Michael Greeff, and Andreas Krause. Hierarchical image classification using entailment cone embeddings. In *CVPRW*, 2020. **14**

[98] Shaoteng Liu, Jingjing Chen, Liangming Pan, Chong-Wah Ngo, Tat-Seng Chua, and Yu-Gang Jiang. Hyperbolic visual embedding learning for zero-shot recognition. In *CVPR*, 2020. **14**

[99] Chao Jia, Yinfei Yang, Ye Xia, Yi-Ting Chen, Zarana Parekh, Hieu Pham, Quoc Le, Yun-Hsuan Sung, Zhen Li, and Tom Duerig. Scaling up visual and vision-language representation learning with noisy text supervision. In *ICML*, 2021. **14**

[100] Amanpreet Singh, Ronghang Hu, Vedanuj Goswami, Guillaume Couairon, Wojciech Galuba, Marcus Rohrbach, and Douwe Kiela. Flava: A foundational language and vision alignment model. In *CVPR*, 2022. **14**

[101] Lu Yuan, Dongdong Chen, Yi-Ling Chen, Noel Codella, Xiyang Dai, Jianfeng Gao, Houdong Hu, Xuedong Huang, Boxin Li, Chunyuan Li, et al. Florence: A new foundation model for computer vision. *arXiv preprint arXiv:2111.11432*, 2021. **14**

[102] Zirui Wang, Jiahui Yu, Adams Wei Yu, Zihang Dai, Yulia Tsvetkov, and Yuan Cao. Simvlm: Simple visual language model pretraining with weak supervision. *arXiv preprint arXiv:2108.10904*, 2021. **14**

[103] Georgios Pavlakos, Xiaowei Zhou, Konstantinos G Derpanis, and Kostas Daniilidis. Coarse-to-fine volumetric prediction for single-image 3d human pose. In *CVPR*, 2017. **14**

[104] Jiefeng Li, Can Wang, Wentao Liu, Chen Qian, and Cewu Lu. Hmor: Hierarchical multi-person ordinal relations for monocular multi-person 3d pose estimation. In *ECCV*, 2020. **14**

[105] Julieta Martinez, Rayat Hossain, Javier Romero, and James J Little. A simple yet effective baseline for 3d human pose estimation. In *ICCV*, 2017. **14**

[106] Xiao Sun, Jiaxiang Shang, Shuang Liang, and Yichen Wei. Compositional human pose regression. In *ICCV*, 2017. **14**

[107] Hao-Shu Fang, Jiefeng Li, Hongyang Tang, Chao Xu, Haoyi Zhu, Yuliang Xiu, Yong-Lu Li, and Cewu Lu. Alphapose: Whole-body regional multi-person pose estimation and tracking in real-time. *TPAMI*, 2023. **14**

[108] Rıza Alp Güler, Natalia Neverova, and Iasonas Kokkinos. Densepose: Dense human pose estimation in the wild. In *CVPR*, 2018. **14**

[109] Matthew Loper, Naureen Mahmood, Javier Romero, Gerard Pons-Moll, and Michael J Black. Smpl: A skinned multi-person linear model. *TOG*, 2015. **14**

[110] Georgios Pavlakos, Vasileios Choutas, Nima Ghorbani, Timo Bolkart, Ahmed A. A. Osman, Dimitrios Tzionas, and Michael J. Black. Expressive body capture: 3d hands, face, and body from a single image. In *CVPR*, 2019. **14**

[111] Angjoo Kanazawa, Michael J Black, David W Jacobs, and Jitendra Malik. End-to-end recovery of human shape and pose. In *CVPR*, 2018. **14**

[112] Vasileios Choutas, Georgios Pavlakos, Timo Bolkart, Dimitrios Tzionas, and Michael J. Black. Monocular expressive body regression through body-driven attention. In *ECCV*, 2020. **14**

[113] Georgios Pavlakos, Vasileios Choutas, Nima Ghorbani, Timo Bolkart, Ahmed A. A. Osman, Dimitrios Tzionas, and Michael J. Black. Expressive body capture: 3d hands, face, and body from a single image. In *CVPR*, 2019. **14, 19, 26**

[114] Nikos Kolotouros, Georgios Pavlakos, Michael J Black, and Kostas Daniilidis. Learning to reconstruct 3d human pose and shape via model-fitting in the loop. In *ICCV*, 2019. **14**

[115] Hanbyul Joo, Natalia Neverova, and Andrea Vedaldi. Exemplar fine-tuning for 3d human model fitting towards in-the-wild 3d human pose estimation. In *3DV*, 2021. **14**

[116] Ben Mildenhall, Pratul P. Srinivasan, Matthew Tancik, Jonathan T. Barron, Ravi Ramamoorthi, and Ren Ng. Nerf: Representing scenes as neural radiance fields for view synthesis. In *ECCV*, 2020. **14**

[117] Chung-Yi Weng, Brian Curless, Pratul P. Srinivasan, Jonathan T. Barron, and Ira Kemelmacher-Shlizerman. HumanNeRF: Free-viewpoint rendering of moving people from monocular video. In *CVPR*, 2022. **14**

[118] Nishant Rai, Haofeng Chen, Jingwei Ji, Rishi Desai, Kazuki Kozuka, Shun Ishizaka, Ehsan Adeli, and Juan Carlos Niebles. Home action genome: Cooperative compositional action understanding. In *CVPR*, 2021. **15, 16**

[119] Z. Cao, G. Hidalgo Martinez, T. Simon, S. Wei, and Y. A. Sheikh. Openpose: Realtime multi-person 2d pose estimation using part affinity fields. *TPAMI*, 2019. **15**

[120] V. Delaitre, I. Laptev, and J. Sivic. Recognizing human actions in still images: a study of bag-of-features and part-based representations. In *BMVC*, 2010. **16, 20**

[121] Mohammad Amin Sadeghi and Ali Farhadi. Recognition using visual phrases. In *CVPR*, 2011. **16**

[122] Bangpeng Yao, Xiaoye Jiang, Aditya Khosla, Andy Lai Lin, Leonidas Guibas, and Li Fei-Fei. Human action recognition by learning bases of action attributes and parts. In *ICCV*, 2011. **16**

[123] Mykhaylo Andriluka, Leonid Pishchulin, Peter Gehler, and Bernt Schiele. 2d human pose estimation: New benchmark and state of the art analysis. In *CVPR*, 2014. **16**

[124] Jingen Liu, Jiebo Luo, and Mubarak Shah. Recognizing realistic actions from videos “in the wild”. In *CVPR*, 2009. **16**

[125] Khurram Soomro, Amir Roshan Zamir, and Mubarak Shah. Ucf101: A dataset of 101 human actions classes from videos in the wild. *arXiv preprint arXiv:1212.0402*, 2012. **16**

[126] Juan Carlos Niebles, Chih-Wei Chen, and Li Fei-Fei. Modeling temporal structure of decomposable motion segments for activity classification. In *ECCV*, 2010. 16

[127] Weiyu Zhang, Menglong Zhu, and Konstantinos G Derpanis. From actemes to action: A strongly-supervised representation for detailed action understanding. In *ICCV*, 2013. 16

[128] Gunnar A Sigurdsson, Abhinav Gupta, Cordelia Schmid, Ali Farhadi, and Karteek Alahari. Actor and observer: Joint modeling of first and third-person videos. In *CVPR*, 2018. 16, 20

[129] Hang Zhao, Zhicheng Yan, Lorenzo Torresani, and Antonio Torralba. Hacs: Human action clips and segments dataset for recognition and temporal localization. *arXiv preprint arXiv:1712.09374*, 2019. 16

[130] Chen Chen, Roozbeh Jafari, and Nasser Kehtarnavaz. Utd-mhad: A multimodal dataset for human action recognition utilizing a depth camera and a wearable inertial sensor. In *ICIP*, 2015. 16

[131] Ilya Loshchilov and Frank Hutter. Decoupled weight decay regularization. *arXiv preprint arXiv:1711.05101*, 2017. 20

[132] Ekin Dogus Cubuk, Barret Zoph, Dandelion Mané, Vijay Vasudevan, and Quoc V. Le. Autoaugment: Learning augmentation policies from data. *CorR*, abs/1805.09501, 2018. 21

[133] Shen Yan, Xuehan Xiong, Anurag Arnab, Zhichao Lu, Mi Zhang, Chen Sun, and Cordelia Schmid. Multiview transformers for video recognition. In *CVPR*, 2022. 21

[134] Jiahui Yu, Zirui Wang, Vijay Vasudevan, Legg Yeung, Mojtaba Seyedhosseini, and Yonghui Wu. Coca: Contrastive captioners are image-text foundation models. *arXiv preprint arXiv:2205.01917*, 2022. 21

[135] Robert Geirhos, Kantharaju Narayananappa, Benjamin Mitzkus, Tizian Thieringer, Matthias Bethge, Felix A Wichmann, and Wieland Brendel. Partial success in closing the gap between human and machine vision. *NeurIPS*, 2021. 23

[136] Thomas Lucas\*, Fabien Baradel\*, Philippe Weinzaepfel, and Grégory Rogez. Posegpt: Quantization-based 3d human motion generation and forecasting. In *ECCV*, 2022. 23

[137] Georgios Pavlakos, Vasileios Choutas, Nima Ghorbani, Timo Bolkart, Ahmed A. A. Osman, Dimitrios Tzionas, and Michael J. Black. Expressive body capture: 3d hands, face, and body from a single image. In *CVPR*, 2019. 28

[138] Shuhuai Ren, Lei Li, Xuancheng Ren, Guangxiang Zhao, and Xu Sun. Rethinking the openness of clip. *arXiv preprint arXiv:2206.01986*, 2022. 28

[139] Anish Acharya, Sujay Sanghavi, Li Jing, Bhargav Bhushanam, Dhruv Choudhary, Michael Rabbat, and Inderjit Dhillon. Positive unlabeled contrastive learning. *arXiv preprint arXiv:2206.01206*, 2022. 28

We report more details and analyses here:

- Sec. A: Supplementary Related Works
- Sec. B: More Details of *Pangea* Database
- Sec. C: More Details of P2S
- Sec. D: More Details of S2P
- Sec. E: Datasets Details in Experiments
- Sec. F: Implementation Details
- Sec. G: Detailed Analysis of Transfer Learning
- Sec. H: Additional Results of P2S and S2P
- Sec. I: Additional Ablation Studies
- Sec. J: More Discussions

## A. Supplementary Related Works

### A.1. Hyperbolic Representation

Hyperbolic representation has emerged in deep learning to encode hierarchical tree-like structure and taxonomy [77, 93, 94]. It has been applied in computer vision for hierarchical action search [59], video action prediction [95], and hierarchical image classification [96, 97, 98]. Long *et al.* [59] project video and action embeddings in the hyperbolic space and train a cross-modal model to perform hierarchical action search. In this work, we use hyperbolic embeddings to encode the hierarchical geometry of our structured semantic space.

### A.2. Visual-Language Learning

Visual-language learning recently shows potential in learning generic representations [11, 99, 100, 101, 102]. Specifically, CLIP [11] and ALIGN [99] benefit from web-scale curated image-text pairs for training and allow zero-shot transfer to many downstream tasks. Following works [92, 85] adapt CLIP to video recognition via prompting, temporal modeling, *etc.* However, their implicit language embedding may be hard to capture the subtle taxonomy and structure knowledge of action semantics. Thus, we propose to solve the problem via a structured semantic space.

### A.3. 3D Human Representation

3D Human Representation has been attracting much attention for a long time. A most intuitive representation is the 3D human pose, and lots of effort has been put into single-view 3D pose reconstruction [103, 104, 105, 106]. Some methods [103, 106] directly regress 3D pose from the given image. While given the great progress in 2D pose estimation [107], many works [104, 105] adopt pre-detected 2D poses as auxiliary inputs. DensePose [108] proposes to adopt a UV map to represent the dense correspondence between the image and a human mesh, which could function as a 2.5D human representation. Lately, different parametric human body models (like SMPL [109] and SMPL-X [110]) are proposed as promising human representations.

Impressive performance has been achieved with weak supervision, like 2D pose [111, 109, 110, 112, 72], semantic segmentation, motion dynamics, and so on. Also, different paradigms are proposed. Some works [70, 113] directly fit the parametric model to the weak supervision signals, which is accurate but sensitive to the initial state, and the speed is restricted. While there are also regression methods [111, 112, 72] learning a neural network to map images to human model parameters, greatly accelerating the reconstruction but losing accuracy. Combing the advantages of both kinds of methods, SPIN [114] and EFT [115] proposed to adopt regression methods for initialization and then use fitting methods for refinement. Inspired by the recent progress in NeRF [116], HumanNeRF [117] proposed a neural radiance field representation for free-view dynamic human modeling.

## B. More Details of *Pangea* Database

### B.1. Data Curation

With the structured semantic space, We can collect data with diverse modalities, formats, and granularities, and adapt them into a unified form. Our database *Pangea* contains a large range of data including image, video, and skeleton/MoCap. We give more details of the processing and formulation as follows:

**1) Semantic consistency.** The class definitions in datasets are various, but they can be mapped to our broad coverage semantic space with the fewest semantic damages. The mapping is completed via crowd-sourced annotation with the help of word embedding distances. Only *one-time alignment* is required for a dataset. As more and more classes are aligned and covered, the process would be faster and faster with synonyms checking. Please refer to Suppl. Sec. B.2 for details.

**2) Temporal consistency.** Some videos [4] only have *sparse* labels for a whole clip instead of each frame. To solve this conflict, we sample the clip with *3 fps* and give them the label of their belonged clip describing the action during the clip. More dense or spare sampling is either computationally costly or with serious information loss. On the contrary, with *dense* frame labels [20], we can easily get the clip label via fusing frame labels. Thus, we provide both frame- and clip-level labels for videos.

**3) Spatial consistency.** There are both instance (boxes) [27] and image [8] level labels. It is too expensive to annotate all missing human boxes and actions to make the whole *Pangea* instance-level. More realistically, we merge the instance labels of each image/frame into image/frame labels. In the future, we can also add more box labels to existing images based on the existing instance labels to support larger-scale instance-level training.

**4) 3D format consistency.** 3D action datasets typically

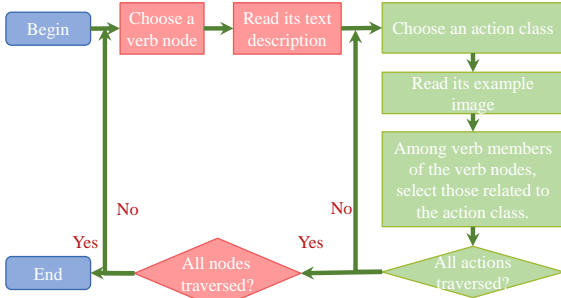


Figure 9: The flow chart of the action semantic mapping.

have different formats, *e.g.*, SMPL [70] contains 24 key-points while CMU MoCap [6] has 31 key-points. To keep format consistency, we transform all of them into SMPL via a fitting procedure.

**5) 2D-3D consistency.** Image/video datasets mostly contains only 2D labels without 3D human labels. We generate 3D humans via single-view reconstruction [72]. Please refer to Suppl. Sec. B.3 for more details.

## B.2. Action Semantic Mapping Details

Suppl. Fig. 9 shows a flow chart of the action semantic mapping. To achieve semantic consistency, various classes of the collected datasets are first mapped to our semantic space for unified labeling. As a dataset usually contains limited classes, we manually align them to the underlying verb nodes via crowd-sourced annotation. Only **one-time alignment** is required for a dataset. As more and more classes are aligned and covered, the process would be faster and faster with synonyms checking.

Given action class set  $A = \{a_i\}_{i=1}^p$  and verb node set  $M = \{m_j\}_{j=1}^n$ , where the  $j$ -th node  $m_j$  has its verb members  $m_j^k$ , *i.e.*,  $m_i = \{m_j^k\}_{k=1}^{n_j}$ . Through semantic mapping, we establish the relation  $R = \{(a_i, m_j^k) | (a_i, m_j^k) \in \{0, 1\}\}$ , *i.e.*, the semantic correlation between each class and verb members. For each node (*e.g.*, push-12-1-1), the annotator first read the text descriptions to understand their meanings. Also, all the verb members of this node are listed. Next, for each candidate class (*e.g.*, squeeze sponge from [118]), the annotator needs to select verb members related to it. Example images were given to help the understanding. Considering the sheer number of classes (4 K+ total), we filter out the unrelated classes for each node beforehand. For a verb node  $m_j$ , we calculate its *semantic distance* with all  $p$  classes as  $D_j = \{\min_{1 \leq k \leq n_j} \mathcal{D}(a_i, m_j^k)\}_{i=1}^p$ , *i.e.*, choose action classes with closer semantic distance  $\mathcal{D}(\cdot, \cdot)$  with its verb members. In practice,  $\mathcal{D}(\cdot, \cdot)$  is instantiated as the cosine distance of Bert vectors [12]. According to the manual trivial-and-error, we find that picking the top 25% classes as candidates is ac-

curate enough as the selection reference, which can reduce the workload significantly. We invite 60 annotators of different backgrounds. Each candidate class is annotated three times, generating the final labels via the majority rule. Finally, for the 898 verb nodes (including 575 leave nodes), there are a total of 515 verb nodes that have corresponding retargeted classes (including 290 leave nodes). The missing verb nodes are mostly related to visually unrecognizable semantics, *e.g.*, invest.

## B.3. 3D Human Body Annotation Details

We adopt 3D humans for multiple reasons. First, 3D human provides a robust representation without *viewpoint* problems. Second, the 3D human can be seen as the safest choice as the physical carrier of actions with no need of considering the *domain gap* across image conditions.

In *Pangea*, we also prepare pseudo 3D human labels for images/videos. Different strategies are adopted depending on the label circumstances of the data. For different scenarios with ground truth (GT) 2D or 3D human poses, human boxes only, and no human instance labels at all, we adopt different strategies as follows:

1. If an image has the 3D human pose annotation, we fit the SMPL model to the 3D pose and associate the fitted 3D human body with the annotation. The 2D body is acquired by cropping the image with the bounding box.
2. If an image has the 2D human pose annotation, we calculate the MSE error of the annotated pose and the re-projected pose from 3D recovering and associate the annotated human instance with the reconstructed 3D body whose MSE error is the lowest among all and lower than a threshold. The 2D body representation is acquired by cropping the image with the box.
3. If an image has the human bounding box annotation, we calculate the IoU between the annotated box and the re-projected human mesh bounding box. Then, the annotated human box is associated with the 3D human body whose IoU is the highest and higher than a threshold. The 2D body representation is acquired by cropping the image with the bounding box.
4. If an image contains no human annotation, OpenPose [119] is adapted to generate a pseudo annotation for the 2D human pose. Then we follow the same association strategy as images with 2D pose annotation. And we assume the human instance with the lowest MSE error is the target human performing the annotated action.
5. For mesh sequences, we directly adopt them as 3D humans. Besides, for skeleton sequences without a 2D image available, we align the annotations with joints

		Action Classes	Images/Frames	Videos
Image	Willow Action [120]	7	1 K	-
	Phrasal Recognition [121]	10	1 K	-
	Stanford 40 Actions [122]	40	9 K	-
	MPII [123]	410	14 K	-
	HICO [8]	600	38 K	-
	V-COCO [18]	29	10 K	-
Video	HAKE [34]	156	100 K	-
	HMDB51 [57]	51	41 K	7 K
	HAA500 [9]	500	51 K	10 K
	AVA [20]	80	166 K	0.5 K
	YouTube Action [124]	11	7 K	1 K
	ASLAN [56]	432	30 K	1 K
	UCF101 [125]	101	126 K	13 K
	Olympic Sports [126]	16	16 K	1 K
	Penn Action [127]	15	95 K	2 K
	Charades [89]	157	31 K	10 K
	Charades-Ego [128]	157	235 K	8 K
	ActivityNet [22]	200	1,619 K	20 K
	HACS [129]	200	1,379 K	504 K
	Home Action Genome [118]	453	702 K	6 K
Skeleton/MoCap	Kinetics [4]	700	5,461 K	215 K
	HumanAct12 [6]	12	90 K	1 K
	CMU MoCap [6]	8	978 K	1 K
	UTD-MHAD [130]	27	90 K	1 K
	NTU RGB+D [7]	120	830 K	114 K
	Human3.6M [5]	17	3,600 K	1 K
	BABEL [25]	260	4,050 K	10 K
Total	HAA4D [91]	300	212 K	3 K
	Pangea	4,712	20,044 K	952 K

Table 10: Statistics of collected and curated multi-modal datasets. Note that different datasets may share part of images/frames (e.g., HICO [8] and HAKE [34]) or action classes (e.g., ActivityNet [22] and HACS [129]).

defined by SMPL and extract the 3D human body by fitting the SMPL model to the aligned pose.

Note that the 3D human pose and the corresponding/re-projected 2D pose could be easily extracted simultaneously. Images/frames with no human bodies or failure reconstructions were dropped. In practice, ROMP [72] and EFT [73] are adopted to directly recover humans from images.

#### B.4. More Statistics of *Pangea*

We list the collected datasets of *Pangea* in Suppl. Tab. 10.

#### B.5. Semantic Distribution of *Pangea*

Suppl. Fig. 10 shows the samples count for 290 leave verb nodes of our *Pangea* database. Detailed statistics on tail/head verb nodes are also listed.

#### B.6. Data License/Address

All the data of *Pangea* are from the open-sourced datasets and for research purposes only. We give the data licenses and links of the gathered datasets here.

- Willow Action: <https://www.di.ens.fr/willow/research/stillactions/>
- Phrasal Recognition: <https://vision.cs.uiuc.edu/phrasal/>
- Stanford 40 Action: <http://vision.stanford.edu/Datasets/40actions.html>
- MPII: <http://human-pose.mpi-inf.mpg.de/>
- HICO: <http://www-personal.umich.edu/~ywchao/hico/>
- V-COCO: <https://www.v7labs.com/open-datasets/v-coco>
- HAKE: <http://hake-mvig.cn/download/>
- HMDB51: <https://creativecommons.org/licenses/by/4.0>
- HAA500: <https://www.cse.ust.hk/haa/LICENSE>
- AVA: <https://creativecommons.org/licenses/by/4.0>
- Youtube Action: [http://www.cs.ucf.edu/~liujg/YouTube\\_Action\\_dataset.html](http://www.cs.ucf.edu/~liujg/YouTube_Action_dataset.html)
- ASLAN: <https://talhassner.github.io/home/projects/ASLAN/ASLAN-main.html>
- UCF101: <https://www.crcv.ucf.edu/data/UCF101.php>
- Olympic Sports: <http://vision.stanford.edu/Datasets/OlympicSports/>
- Penn Action: <http://dreamdragon.github.io/PennAction/>
- Charades: <http://vuchallenge.org/license-charades.txt>
- Charades-Ego: <https://prior.allenai.org/projects/data/charades-ego/license.txt>
- ActivityNet: <http://activity-net.org/download.html>

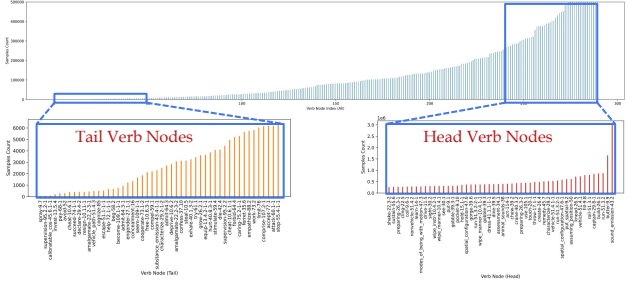


Figure 10: Semantic distribution of samples on 290 leave nodes, including detailed statistics on tail/head verb nodes.

- HACS: <http://hacs.csail.mit.edu/>
- Home Action Genome: <https://homeactiongenome.org/index.html#what-we-do>
- Kinetics: <https://creativecommons.org/licenses/by/4.0>
- HumanAct12: <https://github.com/EricGuo5513/action-to-motion>
- CMU MoCap: <http://mocap.cs.cmu.edu/>
- UTD-MHAD: <https://personal.utdallas.edu/~kehtar/UTD-MHAD.html>
- NTU RGB+D: <https://rosel.ntu.edu.sg/dataset/actionRecognition/>
- Human3.6M: <http://vision.imar.ro/human3.6m/eula.php>
- BABEL: <https://babel.is.tue.mpg.de/license.html>
- HAA4D: <https://cse.hkust.edu.hk/haa4d/>

## C. More Details of P2S

### C.1. Poincaré Ball Construction for Verb Hierarchy

In the verb tree, higher-level summarization of similar human actions would be set as the superior nodes, *i.e.*, the parents or grandparents of the descendant nodes. In training and inference, we can give different levels of granularity supervision and predictions flexibly.

For the tree structure, an intuitive method is to directly classify all nodes via a hierarchical classifier. Directional classification is difficult due to a large number of verb nodes (more than 800 nodes) and hard to apply in the downstream tasks. Thus, we adopt the hyperbolic embedding method and prompt learning to encode the geometric information within *Pangea*. We give more details about the construction of the Poincaré ball here.

In the hyperbolic semantic space, the path from the hypernymy nodes to the hyponym nodes is embedded as a process of continuous change from the Poincaré disk center to its periphery. To train Poincaré ball embeddings, we follow the setting in [77], where the links between verb nodes are provided, and the Riemannian optimizer RSGD is used. We use several constraints to keep the tree structure: (1) The nodes with the same hypernymy should be close; (2) The nodes with different hypernymy nodes should be far away from each other; (3) The shortest path from the node to his sibling should pass their hypernymy node. We train

the embeddings for 600 epochs, with a batch size of 10 and a learning rate of 0.3.

Besides, we also consider Poincaré Glove embeddings [93] for geometry encoding. However, it is constructed based on WordNet vocabulary and improperly represents verbs in VerbNet. Also, the detailed description provided by VerbNet cannot be effectively encoded by Poincaré Glove embeddings for a single word.

### C.2. Semantic Encoding and Alignment

We give a figure to explain the strategies of the semantic encoding and alignment in Suppl. Fig. 11. For the text information of “touch-20-1” (green box), the selected text is “[BOS] grasp pat touch ... manipulation [EOS]”.

### C.3. Label Augmentation Details

We detail the label augmentation here. Each image has a partial annotation  $Y = \{y_i | y_i = 1, 0, \emptyset\}_{i=1}^N$ , where 1, 0 are certain positive/negative labels, and  $\emptyset$  are uncertain ones.

A direct way to solve the uncertain labels is *assuming negative*: unobserved labels are considered as negatives. That is, for  $\forall i$ , if  $y_i = \emptyset$ , assign  $y_i = 0$ . But, some positive labels are falsely treated negatively, which hinders semantic learning, especially for few-shot nodes. Therefore, we propose to generate pseudo labels for uncertain labels, instead of simply treating them as negatives. That is, if  $y_i = \emptyset$ , assign  $y_i = y'_i \in [0, 1]$ . The pseudo label  $y'_i$  is generated based on the structure and language before our semantic space. The pre-defined geometry and semantic information in VerbNet indicate the co-relation between verb nodes. Based on the co-relation, high-quality nodes with more samples can transfer knowledge (positive/negative labels) to low-quality nodes with fewer samples, thus generating pseudo labels to apply label augmentation and facilitate P2S learning. The process is illustrated in Suppl. Fig. 12.

In the implementation, we first obtain a co-relation matrix  $\mathbf{C} = \{c_{ij}\}_{N \times N}$  of  $N$  verb nodes via language priors and VerbNet structure. Then pseudo labels are generated based on  $\mathbf{C}$  and certain labels. That is, for each  $i$  where  $y_i = \emptyset$ , we assign  $y'_i = \sum_{j: y_j = 1, j \neq i} c_{ij} y_j$ .

The co-relation matrix  $\mathbf{C}$  is calculated from two components: 1)  $C_L$  based on language priors; 2)  $C_G$  based on VerbNet structure. For  $C_L$ , we encode the semantic information of each verb node into  $l_i$  via a pre-trained text encoder [12] and then construct  $C_{lang} = \cos(l_i, l_j)$ , where  $\cos(\cdot, \cdot)$  measures the cosine similarity of two vectors. For  $C_G$ , based on the trained hyperbolic embeddings  $G = \{g_i\}_{i=1}^N$ , we obtain  $C_G = 1/d(g_i, g_j)$ , where  $d(\cdot, \cdot)$  is the Poincaré distance, and assign  $c_{ij} = 0$  for  $i = j$  to avoid zero division. Finally, we normalize both  $C_L$  and  $C_G$  into  $[0, 1]$  and obtain  $C$  via  $C = (C_L + C_G)/2$ .

With label augmentation, the long-tail distribution is ef-

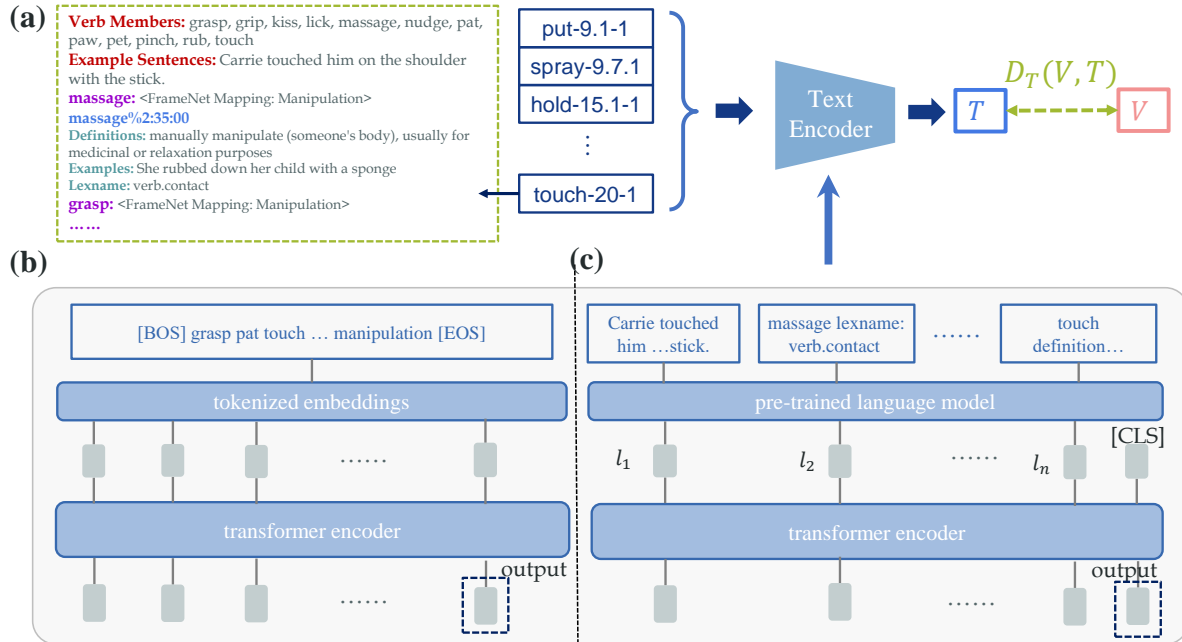


Figure 11: Semantic encoding and P2S mapping from  $V$  to  $T$ . a) Pipeline. Green box: texts of a node case “touch-20-1”. b) Text sampling. c) Pre-trained language vectors.

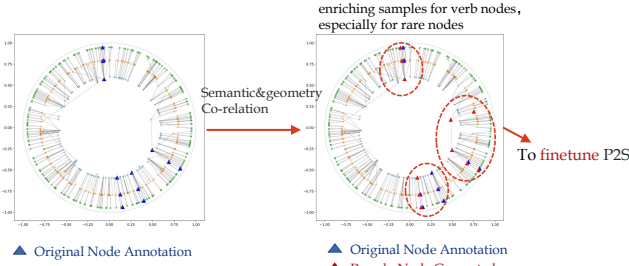


Figure 12: Illustration of label augmentation. Pseudo labels are generated based on VerbNet semantic/geometry co-relation. With generated pseudo labels, we can finetune P2S with more samples, which especially benefits verb nodes with rare samples.

fectively alleviated with credible pseudo labels. The sample distribution before/after generating pseudo labels is shown in Suppl. Fig. 13. We can find that many tail nodes have more samples after the augmentation which alleviate the long-tailed distribution a lot. To benefit from label augmentation, we train P2S mapping in two phases. In phase 1, the whole model is trained via *assuming negative*. In phase 2, we finetune the model with certain labels and pseudo labels. Phase 2 benefits from the eased long-tail distribution, thus facilitating P2S learning.

Another consideration is to bind prediction with **soft** or **hard** pseudo labels. For soft labels, we directly use the pseudo label  $y'_i \in [0, 1]$  as ground truth. For hard labels,

we consider only pseudo labels above the given threshold and use  $y'_i \in \{0, 1\}$  as ground truth. We find hard labels drag the performance a little, possibly because of the amplified noise of generated pseudo labels. Thus, we adopt soft labels in practice.

## D. More Details of S2P

We demonstrate more details of our S2P learning model. The model is illustrated in Suppl. Fig. 14. We follow a cVAE structure, where two MLPs are adopted as human encoder and decoder. The geometry encoder and text encoder from the P2S model are used to encode the semantic information into conditions. During training, the standard KL divergence loss and reconstruction loss are imposed.

## E. Datasets Details in Experiments

**HICO** [8] is an *image-level* benchmark for Human-Object Interaction (HOI) recognition. It has 38,116 and 9,658 images in the train and test sets and defines 600 HOIs composed of 117 verbs and 80 COCO objects [61]. Each image has an image-level label which is the aggregation over all HOIs in an image without human boxes. We use mAP for multi-label classification.

**HAA** [9] is a video *clip-level* human-centric atomic action dataset. It defined 500 actions and contains 10,000 video clips which are split into 8,000 training, 500 validating, and 1,500 testing clips. Each video clip has one single

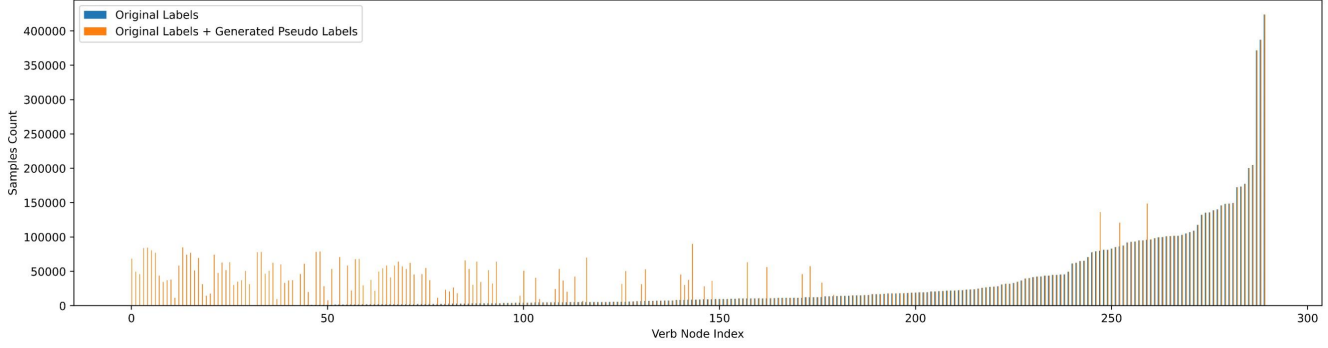


Figure 13: Sample distribution before/after generating pseudo labels.

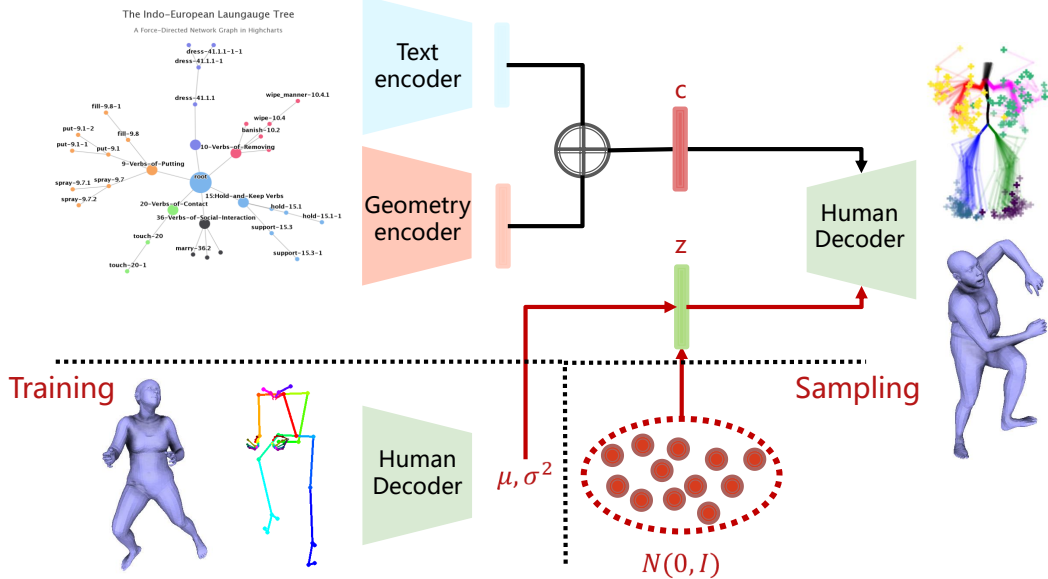


Figure 14: The S2P model structure. An MLP-based cVAE model is adopted, where the geometry encoder and text encoder from the P2S model is used to encode the semantic information into conditions.

action label. The top-1 accuracy metric is utilized for multi-class classification.

**Charades** [89] is a video *frame-level* dataset including everyday activities in 15 indoor scenes with 157 action classes and 30 verbs. We use its frame-wise annotation and evaluate performance with mAP.

**HMDB51** [57] is a video *clip-level* dataset consisting of 6,766 internet videos over 51 classes, and each video has about 20 to 1,000 frames. Each video clip has one single action label. We report the average top-1 accuracy on the standard three splits.

**Kinetics-400** [10] is a video *clip-level* human-focused dataset that includes 240 K training clips and 20 K validation clips over 400 action classes. Each video lasts for about 10 seconds and contains one single label. We report the top-1 accuracy and top-5 accuracy on the official validation set as the convention.

**BABEL** [25] is a large-scale 3D action dataset covering a wide range of human motions, including over 250 unique action classes. It is built upon AMASS [67] by annotating the sequences with *sequence-level* and *frame-level* action classes, represented with the SMPL/SMPL-X body model [70, 113]. Over 43.5 hours of MoCap data is provided with 28,033 sequence labels and 63,353 frame labels and is categorized into one of 260 action classes. We follow the evaluation protocol of BABEL-120 under the Dense label only setting, containing a span of MoCap sequences belonging to 120 classes, where 13,320 sequences are divided into the train (60%), val (20%), and test (20%) sets. A motion-capture span of 5 seconds or less is given, and our model is required to predict the actions in it. Top-1 accuracy is reported. To show our ability in the long-tail classes, the Top-1-norm (the mean Top-1 across classes) is also reported. We adopt the PointNet++ [74] trained on *Pangea*

as initialization and fine-tune it on BABEL. Note that the BABEL-120 benchmark is based on motion sequences. To adapt our model to the setting, we down-sample the original sequence from 60 FPS to 3 FPS, perform inference on all the down-sampled frames, and use *mean pooling* to acquire the final score.

**HAA4D** [91] is an extension of HAA [9]. 3,300 videos of 300 human atomic action classes from HAA are selected to construct a class-balanced and diverse dataset. Each video is annotated with globally aligned 4D human skeletons. While we follow the conventional action classification setting and data split [91]. For classes containing 20 samples, the first 10 samples are adopted for training, and the rest are used for inference. For classes containing 2 samples, the one with a bigger index is adopted for training, while the other one is adopted for inference. We adopt the PointNet++ [74] pre-trained on *Pangea* as the initialization and finetune it on HAA4D. Since HAA4D only provides 4D skeletons, we fit the provided skeletons with SMPL [70] and used the SMPL parameters for training and inference. We perform inference on all the down-sampled frames and use *mean pooling* to acquire the final score.

## F. Implementation Details

We give more implementation details here.

### F.1. P2S Model

(1) For images/frames, we detail the data utility below. For the convenience of expression, we represent our *Pangea* database in Suppl. Tab. 10 into 4 splits: 1) Willow Action [120] ~ HAKE [34]: image datasets; 2) HMDB51 [57] ~ Charades [89]: video datasets with relatively small scale; 3) Charades-Ego [128] ~ Kinetics [4]: video datasets with relatively large scale; 4) HumanAct12 [6] ~ HAA4D [91]: skeleton/MoCap datasets.

We select images from split 1&2 to construct *Pangea* test set to represent verb node semantics. The remaining 10.7 M images are used for training. We first train P2S with split 1&2 data (split 3 is currently excluded to avoid the image domain gap). Then we tune P2S with split 1&2&3 data, where richer samples can facilitate P2S learning.

We use a CLIP pre-trained ViT-B/32 image encoder to extract visual features with a resolution of 224. An AdamW [131] optimizer with a weight decay of 0.05 is used in training. We first use split 1&2 data to train the model for 30 epochs with a batch size of 64. The learning rate is warmed up from 5e-7 to 1e-5 for the initial 2 epochs, then decayed with a cosine scheduler. Then we use split 1&2&3 data to finetune the model for 10 epochs with a batch size of 64 and a learning rate of 1e-6. To benefit from label augmentation, we finetune the model with pseudo labels.

(2) For 3D human point clouds, we use PointNet++ [74] as the encoder. An AdamW [131] optimizer with a weight

decay of 0.05 is used. The model is trained for 100 epochs with a batch size of 128. The learning rate is warmed up from 5e-8 to 2e-6 for the initial 2 epochs, then decayed with a cosine scheduler. For P2S learning, we use 601 K 3D training human instances and test the model on *Pangea* test set with 172 K 3D human instances. About 75% of the human instances are obtained from single-view reconstruction [72, 73]. We adopt GT 3D human for BABEL [25] and use reconstructed 3D human for other datasets.

### F.2. P2S Transfer Learning

P2S pre-trained on *Pangea* with node classification is a knowledgeable **backbone** and can be used in transfer learning. There are three stages in transfer learning: a) Training P2S on *Pangea* following the same setting as above P2S learning, but with the train & test sets of the downstream target dataset **excluded** following a strict transfer learning setting. b) Finetuning P2S on the target dataset train set. c) Testing the finetuned P2S on the target dataset test set. For video benchmarks, we adopt lite implementations for temporal encoding and do not use video augmentation methods. For the simplest temporal coding, we cut out fixed 8 frames for each video clip and *average* logits of 8 frames as the clip logit. We compare several simple temporal coding methods on HAA [9] transfer learning.

- Average prediction of frames. In training, supervision is applied to each frame. In testing, predictions of 8 frames are *averaged* as the clip prediction. Our P2S achieves 68.76% acc with this temporal encoding.
- Mean pooling. Frame-level visual features are first extracted, and the clip-level visual feature is obtained via simple mean pooling of frame-level ones. In training, supervision is applied to each clip. In testing, the clip prediction is directly outputted. With feature mean pooling, our P2S achieves 69.73% acc.
- Temporal transformer. It is operated similarly to the “mean pooling” method, other than a temporal transformer inserted before the mean pooling of frame-level features. With the temporal transformer, our P2S achieves 70.47% acc.

From the above results, we can find that with a more sophisticated model, the performance is higher too. In future work, we believe a larger model with more computation power support will achieve more significant performance improvements with our *Pangea*. In this work, we report P2S results with *average prediction of frames* temporal encoding for simplicity. Even with a very simple temporal encoding, P2S performs comparably with some spatio-temporal (ST) methods. Meanwhile, for the visual encoder, our model is **2.95** GFLOPs, while the SOTA model EVL [85] is **25.96** GFLOPs, which verifies the efficiency of our method. Thus,

P2S can also be used as a *plug-and-play*, we report the results of fusing P2S with SOTA video models.

Especially, since HICO [8] is an image-based benchmark, it suffers from a domain gap with video-based datasets. Thus, we only use split 1&2 data (with HICO [8] data excluded) when pre-training P2S for HICO [8]. The image-based split 1 has a smaller domain gap, thus being the most useful. Small video-based split 2 can also help via increased samples. We do not adopt split 3 to avoid the huge domain gap.

### F.3. S2P Model

S2P is built as a cVAE, where the encoder and decoder are implemented as a 2-layer MLP. The text encoder and geometry encoder in P2S are adopted to encode the semantic information into conditions, which are *frozen* during S2P. The model is trained on *Pangea* using an Adam optimizer for 100 epochs, with a batch size of 256. The learning rate is warmed up from 5e-8 to 2e-6 for the initial 2 epochs and then decayed with a cosine scheduler.

## G. Detailed Analysis of Transfer Learning

### G.1. HICO

On HICO [8], given the image-text pairs from *Pangea*, *CLIP-Pangea* outperforms *CLIP* with 1.3 mAP, verifying the effectiveness of our wide range *Pangea*. However, *CLIP-Pangea* cannot utilize the extensive semantic-geometric knowledge and the structured semantic space. Thus, P2S further boosts the performance and outperforms RelViT and *CLIP* with **8.4** and **2.4** mAP respectively.

We find that HICO [8] designed for human-object interaction (HOI) recognition (verb-object, *e.g.*, `sit_on-chair`) is more difficult than common action recognition (verb, *e.g.*, `sitting`). Moreover, most of *Pangea* data are videos and thus have a larger domain gap with HICO. Thus, compared with other video-based benchmarks, HICO [8] benefits less from P2S pre-training.

### G.2. HAA

On HAA [9], baseline *CLIP* achieves 63.33% Acc. With *CLIP* pre-trained on *Pangea*, more abundant action knowledge is encoded. Thus, *CLIP-Pangea* outperforms the *CLIP* with **3.87%**. P2S further outperforms *CLIP-Pangea* with 1.53% with structured verb node encoding. Besides, as our method adopts a lite setting without heavy temporal encoding and frame augmentation, we also fuse our method with SOTA spatial-temporal method EVL [85] for a fair comparison. The performance of 79.80% further verifies the effectiveness of our method.

Moreover, we also use only a part of HAA training data in stage b) for *CLIP* and P2S. The results are shown in

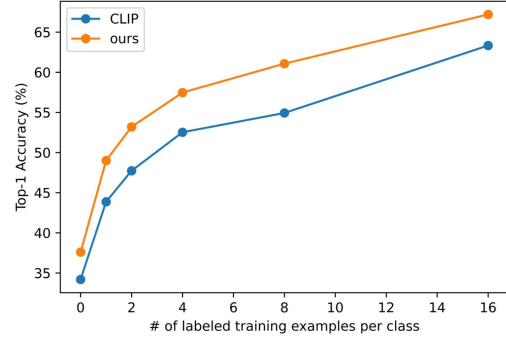


Figure 15: Performance on HAA with partially training data.

Suppl. Fig. 15. We can find that our P2S still obviously outperforms *CLIP* with only a part of HAA training data (*e.g.*, 12.5%, 25%, 50% training data), verifying the effectiveness of P2S.

### G.3. HMDB51

HMDB51 [57] is a popular video benchmark for human action recognition. We utilized the average score of the top-1 accuracy for the standard three splits of HMDB. In consideration of parameter-lite and similar *CLIP*-based architecture, we choose the latest and fully open-sourced EVL [85] for fusion. The baseline *CLIP* scored 63.49%, and *CLIP-Pangea* scored 0.99% higher than *CLIP*. Using our method, P2S scores 65.99% and outperforms *CLIP* by **2.50%**. When fusing with EVL [85], our results boosted the performance of EVL [85] by **3.86%**.

### G.4. Charades

For SOTA methods on Charades [89], we reproduce the fully open-sourced SOTA MoViNet [88]. In fusion, we choose MoViNet-A5 instead of the heavier -A6 which ensembles an -A5 model and an -A4 model. Moreover, to simplify the training, we do not use AutoAugment [132], a technique used in MoViNets to sample a random image augmentation for each video and apply the same augmentation for each frame. The baseline *CLIP* is designed in a way similar to HICO. When compared to *CLIP*, *CLIP-Pangea* scored **2.88** mAP higher, which proves the effectiveness of our *Pangea* database. Furthermore, P2S outperforms *CLIP-Pangea* by an extra **3.22** mAP. When fusing with MoViNet-A5, P2S boosts the performance of -A5 by **7.36** mAP, reaching **60.55** mAP.

### G.5. Kinetics-400

Kinetics-400 [10] is a widely-used dataset in the field of video action recognition. SOTA methods of this benchmark are MTV [133] and CoCa [134]. However, due to the high computation cost and unavailable extra training data, we fail to reproduce their results. Therefore, we choose

the most accessible leading approach EVL [85] for comparison. Another reason is that it is also a CLIP-based and relatively lite method without many spatial or temporal crops. We reproduce its results with the official code and open source model and achieve 87.64% top-1 accuracy and 97.71% top-5 accuracy, which is similar to the reported scores in the paper. Here, we fuse P2S with the reproduced EVL. We conduct experiments with the same two baselines, *CLIP* and *CLIP-Pangea*. Compared to *CLIP* on top-1 accuracy, *CLIP-Pangea* and P2S score 0.25% and 1.93% higher respectively. When fusing with EVL (ViT-L/14) [85], our verb node knowledge boosts the performance by 1.41% and 0.19% on top-1 and top-5 accuracy, narrowing the gap to the larger and heavier SOTA methods.

Besides, only 27.7% data of Kinetics-400 are covered in our current version of *Pangea*, and we *exclude* them in the pre-training for strict transfer learning. Relatively, the train set of Charades only accounts for 0.23% in *Pangea*. Thus, excluding the data of Charades in pretraining has little impact to the long-tailed data distribution and pre-training. This explains the relatively small bonus of P2S on Kinetics-400 [10].

## G.6. BABEL

To show the strength of P2S, we further conduct transfer learning on a large-scale 3D action dataset BABEL [25]. We compare our method with the BABEL official baseline [25]. We adopt 2s-AGCN as the baseline following BABEL [25], which utilizes temporal information. Besides, we use *PointNet++* and *CLIP* as extra baselines. Surprisingly, we find that the simple pipeline *PointNet++* considerably outperforms its counterpart 2s-AGCN. On one hand, we find that the baseline *CLIP* performs not well. The reason may be that, without enough 3D pre-training data, the image-based *CLIP* cannot adapt to the domain of BABEL well. This can be verified that *CLIP-Pangea* performs much better and even outperforms *PointNet++-Pangea* with the help of 3D pre-training samples from *Pangea*. On the other hand, *PointNet++* performs much more robustly than *CLIP* as it is designed to encode the 3D point cloud information which suits this task better. However, they all perform worse than our P2S. As shown, P2S without heavy temporal encoding outperforms all baselines. And *PointNet++-Pangea* and *CLIP-Pangea* also show superiorities upon their original setting *PointNet++* and *CLIP* thanks to the extensive knowledge from *Pangea*.

## G.7. HAA4D

Transfer learning is also conducted on the recently proposed 3D action dataset HAA4D [91]. We compare our method with the HAA4D official baseline [91]. The result comparison has a similar conclusion to the one on BABEL. As shown, competitive performance is achieved with

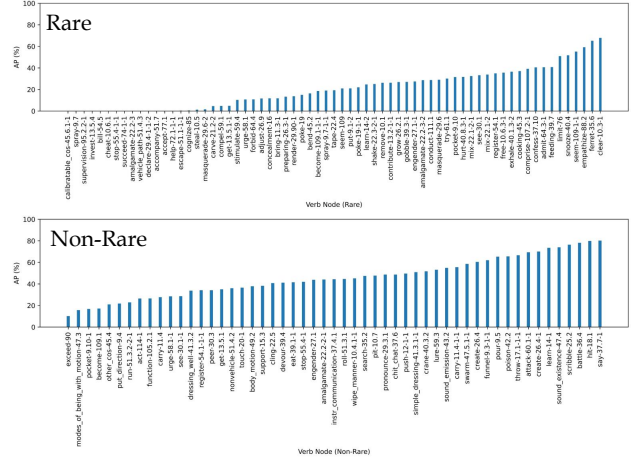


Figure 16: P2S performance on selected rare/non-rare verb nodes on Pangea benchmark. There are a total of 133 rare nodes and 157 non-rare nodes.

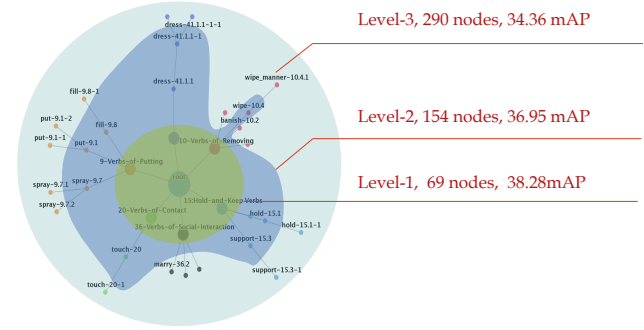


Figure 17: Hierarchical Performance on *Pangea*. We split three levels (green, blue, and cyan for levels 1, 2, and 3) based on the VerbNet hierarchy.

the help of *Pangea* pre-training for *PointNet++* and *CLIP*. Meanwhile, the proposed method such as disentangling, semantic and geometric encoding help P2S further outperform all baselines and SOTA. We also notice that the improvement on HAA4D of P2S upon the SOTA method SGN is relatively smaller. We recognize the reason as two-fold. First, HAA4D provides 3D keypoints as GT annotation, thus we have to fit the SMPL model to the keypoints for the SMPL parameters. This results in noisy inputs for P2S. Second, HAA4D tends to focus more on human atomic body motions. The frames are therefore less discriminative, weakening the performance of our frame-level P2S on HAA4D.

## H. Additional Results of P2S and S2P

### H.1. Action Recognition with P2S

We list performance on selected rare/non-rare verb nodes on *Pangea* benchmark in Suppl. Fig. 16. Our P2S achieves decent performance on both rare and non-rare verb nodes. We visualize the performance of P2S on hierarchical verb nodes in the constructed 2-d Poincaré ball in Suppl. Fig. 17. We can find that the performance of higher levels is higher too, this fits out the intuition that finer-grained actions are more difficult to recognize or have fewer training samples.

Our hierarchical representation is more interpretable. We give a visualization to fully show the ability of P2S to detect **continuous semantic transitions**. For ease of reading, we also list it here in Suppl. Fig. 18. In Suppl. Fig. 18, a detailed analysis is given. P2S can effectively capture the *newly appeared* verbs (e.g., “fill-9.8, knead-26.5”) and *disappeared* verbs (e.g., “knead-26.5”), thanks to the structured semantic space which makes the clearer definition of actions. This confirms our thought that our framework can facilitate coarse-to-finer-grained action understanding.

Suppl. Fig. 19 illustrates two examples of images and predicted verb node logits from *Pangea* test set. For each leave node with high prediction, its verb members and parent node are shown.

### H.2. P2S Consistency Analysis

To measure the model robustness of models, we carry out a consistency test. We follow the setting of [135] and choose 100 head nodes from *Pangea*. For each node, we choose 20 positive image samples and 20 negative samples. The negative samples are chosen from images of other nodes randomly. Each image has undergone **17 transformations**. The first 13 transformations are color-related: grayscale, low contrast, noisy, salt and pepper noise, eidolon, false colour, highpass, lowpass, phase scrambling, power equalization, rotating 90 degrees, rotating 180 degrees, and rotating 270 degrees. The last 4 transformations are style changing, edge extracting, human parsing, and surreal. For the so-called surreal transformation, we grab a constructed 3D human mesh from one image and paste it into another background.

Given the results of our method and the baseline *CLIP*, we make an evaluation based on the metrics proposed in [135] and calculate the **observe consistency** and **error consistency**. Observe consistency and error consistency are calculated about every node. For every node, the observed consistency is near or over 60%, the error consistency is between 20% and 30%. There are three transformations with *striking high* consistency, namely human parsing, eidolon, and surreal. We believe that it is because these three transformations are too difficult. Thus, we take the results of all nodes deleting the 3 weird high-consistency transforma-

tions. The final results are shown in Suppl. Fig. 20.

We can find that on both observed and error consistencies, our method P2S all performs better than *CLIP*. Thus, our method not only achieves better accuracy on recognition but also performs more robustly.

### H.3. 3D Human Pose Generation with S2P

We further visualize more results of S2P in Suppl. Fig. 21.

In detail, we align the samples by the pelvis joint, eliminate the root rotation along the z-axis to make the face orientation consistent, and draw skeletons for 100 samples of the *same node* in the same figure to show the sample distribution. As illustrated, S2P is capable of generating reasonable poses for various nodes. And different nodes hold different geometric characteristics. For example, *ride* poses have elbows away from the spine; *sit* poses tend to have elbows near the spine; While there appears to exist more limb contraction for *kneel* and *sleep*. Also, sample generation of node combination is accessible. By adding the condition *cellphone* upon *sit*, the wrist of the generated samples is restricted to distribute around the pelvis more. Another interesting example is that adding *walk* upon *hug* amplifies the motion range. We show rare combinations like *kneel* plus *hug*. We also show some failure cases of our S2P in Suppl. Fig 22. As shown, when the node combination becomes more complicated, e.g., combining nodes with a larger semantic gap (Poincaré distance), our S2P could fail to generate accurate 3D actions. Here, we only use a simple cVAE to implement S2P. We believe more advanced models such as Transformer [136] or Diffusion [66] could generate more diverse and realistic 3D actions based on *Pangea*. We leave this to future work.

## I. Additional Ablation Studies

### I.1. Semantic Encoding and Alignment

We conduct ablation studies to compare the performance of different semantic encoding strategies in Suppl. Tab. 11. For text sampling, we use the summarized text provided by VerbNet [13]. As a comparison, we use texts not summarized, e.g., choosing only sentences of verb members and canceling out other sentences. The results are reported in Suppl. Tab. 11 (verb members/example sentences/WordNet definition only). We find that the summarized diverse information works better.

The result of the pre-trained language vectors is also shown in Suppl. Tab. 11 (language vectors), which is comparable to text sampling. The possible reason is that there may be a trade-off exists between the encoded text length and learning difficulty. However, given a more powerful large language model [17] to fully utilize the diverse semantic information of verb nodes, things may be different. We

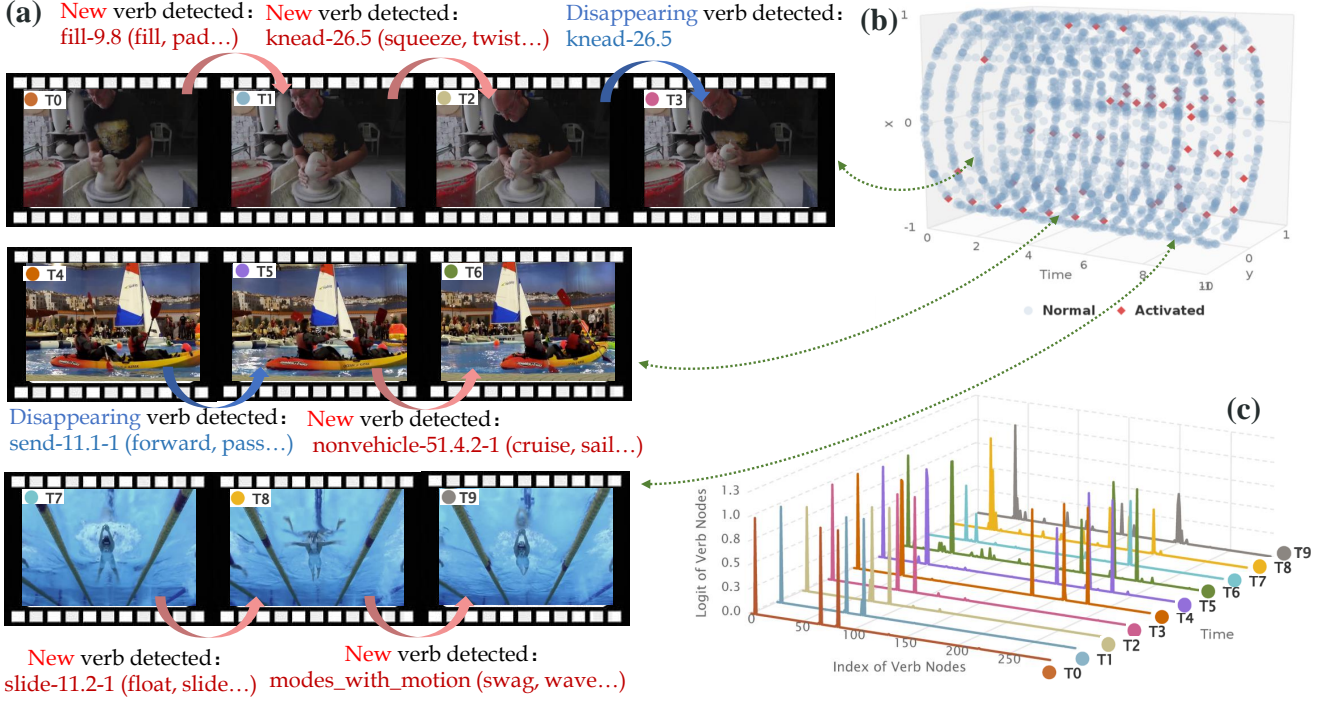


Figure 18: Continuous semantic change. We show the results of 3 videos from the Pangea test set. a) Frames and analysis of the changed node predictions. b) Visualization of predictions of all verb nodes in the Poincaré ball (red: verb nodes with high probabilities). c) Detailed predictions of all verb nodes (peak: verb nodes with high probabilities).

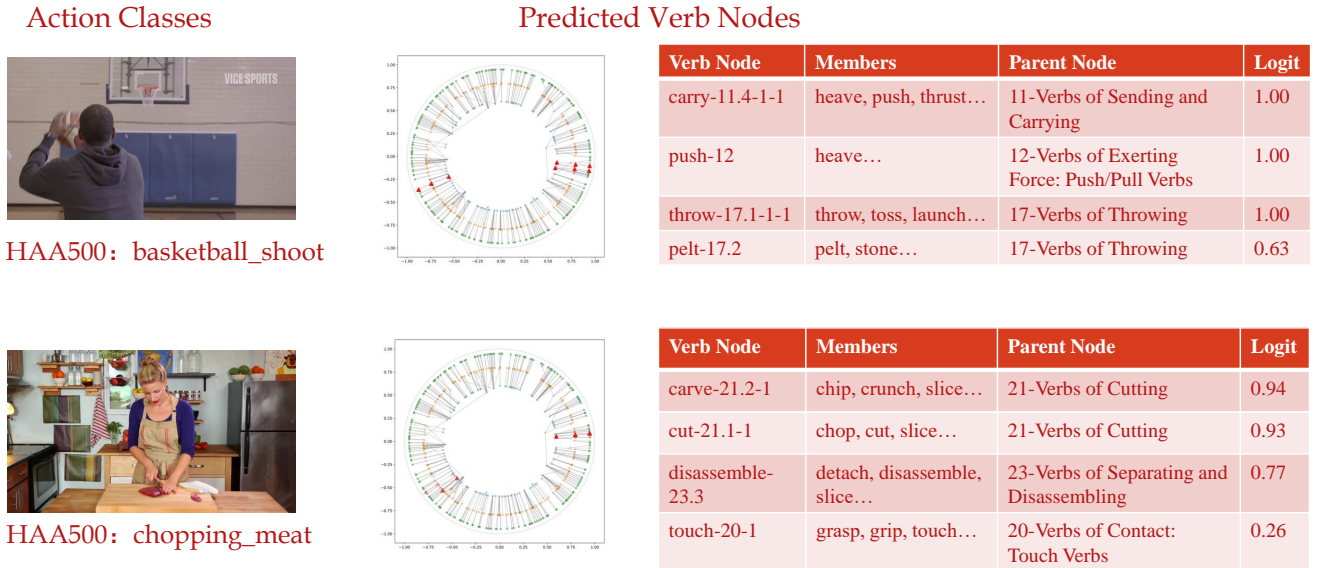


Figure 19: Examples images and predicted verb node logits from the *Pangea* test set.

leave this to future work. We finally choose the summarized text for our P2S model.

## I.2. Geometry Encoding and Alignment

In Suppl. Tab. 12, we show ablation studies of verb node geometry encoding and alignment on *Pangea*. P2S model w/o geometry encoding is given in the first part as a base-

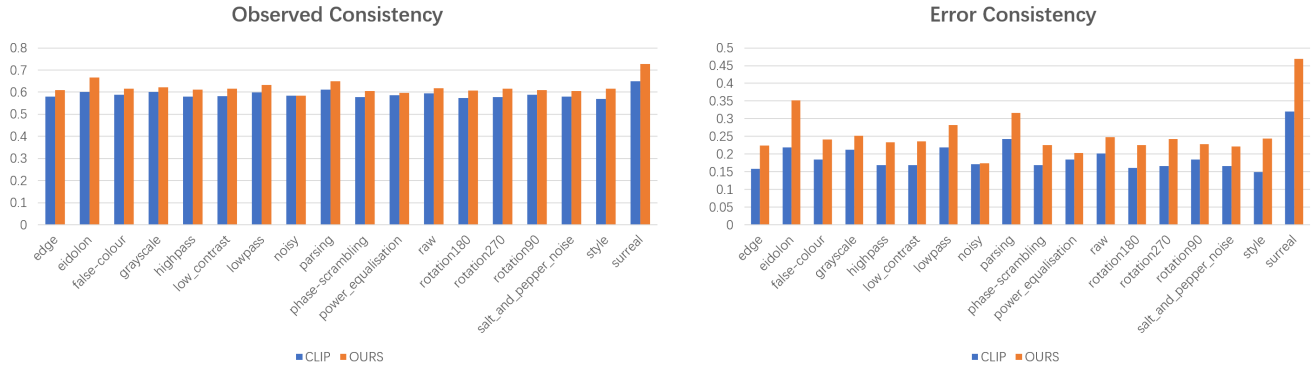


Figure 20: Consistency analysis upon *CLIP* and our method.

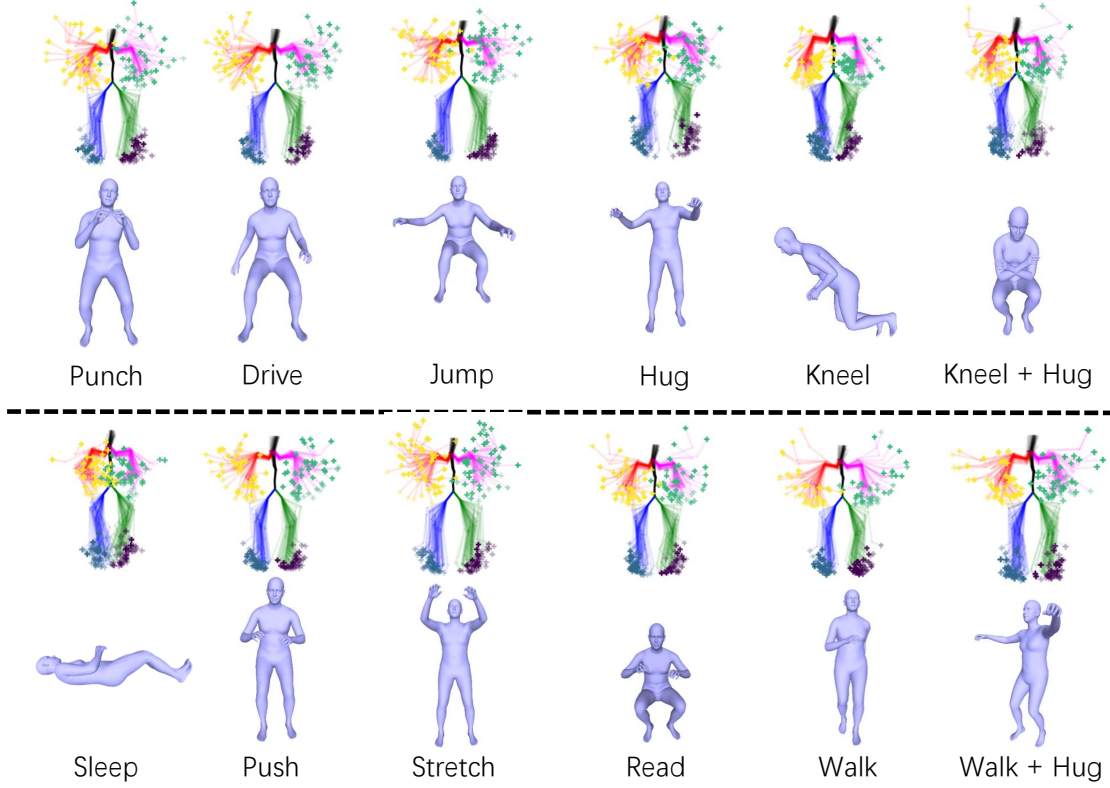


Figure 21: More S2P results.

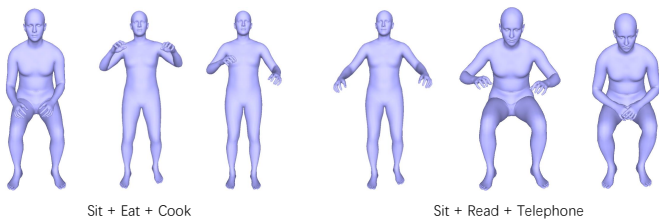


Figure 22: Failure cases of S2P.

Method	Full	Rare	Non-Rare
Summarized Text	<b>34.36</b>	<b>21.75</b>	<b>45.05</b>
Verb Members Only	33.93	21.38	44.57
Example Sentences Only	33.98	21.27	44.75
WordNet Definition Only	33.96	21.20	44.77
Language Vectors	34.32	21.70	45.01

Table 11: Ablation studies of verb node semantic encoding and alignment on *Pangea*.

Method	Full	Rare	Non-Rare
w/o Geometry Encoding	32.89	20.87	43.07
Aligning in Poincare ball	32.43	20.47	42.56
Cross-Domain Mimicking	<b>34.36</b>	<b>21.75</b>	<b>45.05</b>
Geometric Prompt (Text Concatenation)	34.01	21.37	44.72
Geometric Prompt (Prediction Fusion)	<b>36.67</b>	<b>23.36</b>	<b>47.94</b>
Geometric Prompt (Training Alternately)	33.93	21.38	44.57

Table 12: Ablation studies of verb node geometry encoding and alignment on *Pangea*. P2S w/o geometry encoding is first given as a baseline. In the second part, we use hyperbolic embeddings to encode  $G$ , where direct alignment and cross-domain mimicking are compared. In the third part, we use geometric prompt representation and list the three ways to combine  $D_T(V, T)$  and  $D_G(V, G)$ .

line, where it achieves 32.89 mAP. In the second part, we use hyperbolic embeddings to encode  $G$ . With  $V$  reduced the dimension of 2 and compared with hyperbolic embeddings  $G$ , the performance degrades to 32.43 mAP because of the information loss of  $V$ . In contrast, the proposed cross-domain mimicking results in more effective geometry alignment, where  $D_G(V, G)$  is measured via computing pairwise distance matrix without compressing  $V$ .

In the third part, we use geometric prompt representation and list the three ways to combine  $D_T(V, T)$  and  $D_G(V, G)$ . For text concatenation, we concatenate the sentences of semantic and geometric information and input them together into a single text encoder and get representation  $TG$ . We find it outperforms the model w/o geometry encoding but is inferior to cross-domain mimicking. For prediction fusion, two models are trained to align  $V - T$  and  $V - G$  respectively, and the fused prediction achieves 36.67 mAP. It verifies the effectiveness of geometric prompt representation as a powerful supplement to semantic encoding. Besides, training  $T$  and  $G$  alternately degrades the performance a little compared with text concatenation possibly because of the relatively unstable and confusing training.

### I.3. Label Augmentation

Suppl Tab. 13 shows the ablation studies of label augmentation. With label augmentation, P2S-aug outperforms P2S from 34.36 mAP to 34.46 mAP. For pseudo labels generation, we utilize both  $C_L$  and  $C_G$ . When only one type of information is used, P2S-aug shows degraded performance, which verifies the effectiveness of  $C_L$  and  $C_G$ . Currently, the improvement of label augmentation is relatively marginal. The possible reason may be that the rare nodes also have rare neighbors thus there are not enough high-quality generated pseudo labels for rare nodes. In the future, with the supplement for rare nodes specially and a more advanced pseudo label generation method, we believe it would bring more improvements.

Method	Full	Rare	Non-Rare
P2S-aug	<b>34.46</b>	<b>21.84</b>	<b>45.15</b>
P2S	34.36	21.75	45.05
$C_L$ only	34.42	21.80	45.11
$C_G$ only	34.38	21.76	45.08

Table 13: Ablation studies of label augmentation on *Pangea*.

Representation	Method	Full	Non-Rare	Rare
SMPL	MLP	8.32	12.47	3.42
VPoser	MLP	7.81	11.31	2.55
KeyPoints	MLP	5.45	8.44	1.92
Point Clouds	PointNet++	9.16	12.76	3.76
Point Clouds	CLIP	<b>11.57</b>	<b>16.12</b>	<b>6.21</b>

Table 14: Comparison of different 3D representations on the *Pangea* benchmark.

### I.4. 3D Representation in P2S

To find the best feature extractor for 3D action data, we have tried different encoding ways. Specifically, we compared the performance of different representations of the 3D data: (i) SMPL[70] parameters, (ii) VPoser[113], (iii) body keypoints, and (iv) body point cloud. Note that our dataset only contains SMPL parameters, and the other 3 representations are all generated from the SMPL parameters.

For the first 3 representations, we utilize two separate MLPs to encode and classify the 3D data. While for the point cloud, we use the PointNet++[74] as the 3D encoder, with an MLP as the classifier, which is referred to as Pointnet++ in the main text Table 7-8 and Suppl. Tab. 14. Moreover, we also evaluate the CLIP-like classifier, where the cosine similarity between the encoded point cloud feature and the node semantic feature encoded by a text encoder is adopted as the final classification score. This is referred to as *CLIP* in the main text Table 7-8 and Suppl. Tab. 14. Suppl. Tab. 14 shows the results of different 3D representations on the *Pangea* Benchmark. Specifically, in some instances of the *Pangea* dataset, ROMP [72] fails to reconstruct 3D human bodies from the images. For these images, we eliminate these 3D data from the dataset during training and evaluation.

Among these four representations, the point cloud achieves the best results. As for the method, we find that the performance of the model is further improved with a CLIP-like classifier.

We also evaluate the contribution of certain P2S components under the 3D only setting. For example, without disentanglement, the performance degrades to **10.34** mAP, with a considerable performance decline of **2.51** mAP on the Rare set, proving the efficacy of our disentanglement strategy again.

Method	Full	Non-Rare	Rare
Early Fusion	37.08	48.05	24.12
Middle Fusion	36.30	47.37	23.23
Late Fusion	<b>37.55</b>	<b>48.84</b>	<b>24.22</b>

Table 15: Comparison of different multi-modal fusion strategies on the *Pangea* benchmark.

Method	Full	Non-Rare	Rare
CLIP [11]	28.25	37.87	16.90
P2S (2D)	34.46	45.15	21.84
P2S (3D)	11.57	16.12	6.21
P2S (2D+3D)	<b>37.55</b>	<b>48.84</b>	<b>24.22</b>

Table 16: Results of different modality utilization on *Pangea*.

## I.5. 2D-3D Fusion in P2S

We compare different 2D-3D fusion strategies in the P2S model. Note that since *Pangea* contains data from different sources, some of which are not provided with GT 3D human annotation, we adopt ROMP [72] to generate pseudo 3D human annotations. Suppl. Tab. 15 shows the performance comparison of fusing the multi-modal data at different model stages. Early and middle fusion means that we fuse the extracted features of 2D and 3D at the early and middle layers of models respectively. For late fusion, we directly fuse the logits. We can find that the late fusion which directly fuses the outputs of 2D and 3D models performs best.

We also conduct a comparison between 2D only, 3D only, and 2D-3D fusion on *Pangea* in Suppl. Tab. 16. As shown, though P2s with 3D only are not very competitive by themselves, they could still compensate for 2D only and bring considerable improvement.

## J. More Discussions

In this section, we give some discussions about our system and some possible applications and future studies based on our *Pangea* and structured semantic space.

(1) Firstly, we discuss more possible **future applications** of our system as follows:

**New Emergent and Very Rare Actions.** Interestingly, we are creating new actions every day, *e.g.*, new actions such as play VR games, telesurgery given the new inventions like VR player, telesurgery machine. These new emergent actions may have very limited visual and text data. Given our structured semantic space, we can directly align new actions to their related verb nodes efficiently. Then, we can easily find out the related/similar actions from the previous action database robustly instead of teaching machines a new action from scratch. The need for data collection would be largely reduced. Moreover, it could alleviate the difficulty of incremental learning. Fur-

thermore, sometimes it is very hard to collect data for very rare actions (*e.g.*, put out fire), but we can get data easily from its parent, grandparent, or sibling nodes to help us gather its semantics. In inference, different levels of predictions also help because we can enforce their geometry relation consistency to get more robust results.

**Customized Finetuning for Downstream Benchmarks.** We can also customize the pre-train set for each downstream dataset. For example, for AVA, its classes are related to  $n$  nodes in the tree. We can only collect the samples related to these  $n$  nodes in our *Pangea* and their closely-related neighbors to build a customized and more powerful pre-train or train set for AVA.

**Data Usage and Sharing.** Given our *Pangea*, it is easy to add new action data in pre-training or finetuning via the one-time verb node-class alignment. This provides a new solution for future applications to connect the data owner of different domains and fields. In the future, it is also promising to marry *Pangea* and Federated learning to study data sharing and security. Thus, we can build an action data platform to share and fully use data and evaluate the contributions of different data providers and annotators.

**Training Considering Different Verb Tree Levels.** Another possible application is that we can pre-train a model with high-level verb node labels only and then finetune it with finer-grained verb node labels. This follows the learning paradigm from abstract concepts to specific concepts. We leave this to future work.

**Joint Learning of P2S and S2P.** A promising application of our method is to jointly train P2S and S2P. For example, firstly train P2S and get the representative verb node features and then use it in S2P training. Secondly, we can generate new 3D human samples with S2P via distribution sampling. Next, these new 3D human samples can be input into P2S as pseudo samples. During the process, we can gradually add new data with labels to tune two models. This design may construct a loop to connect the bottom-up and top-down models and may show an interesting property. It lays a foundation for better understanding the relationship between human geometry and behavioral semantics.

**Hyperbolic Embedding.** Besides the geometry information encoding, the hyperbolic latent space also acts as an **interpretable indicator** to represent the action semantics and their change in images and videos, which is more than the performance gains. We think this would be vital for future general and interpretable action recognition studies.

**Compositional Complexity.** Human actions have compositional complexity at the human part level. On one hand, we can composite two actions such as eat and walk easily via human body parts control in 3D action generation. On the other hand, this compositionality also brings challenges. Sometimes the label of a sample only reflects the action semantics carried by human parts, *e.g.*, hold by hands, kick

by feet. This phenomenon was studied by HAKE [3, 34] before. Given our structured action semantic space, we may be able to connect human body part states with our verb tree nodes to find out which nodes represent the part-level action semantics and which nodes carry the whole body semantics.

(2) Next, we discuss the **design choices** of our system.

**3D Human.** In our system, we use multi-modal inputs, *i.e.*, 2D image/video and 3D human point cloud from SMPL mesh. Because we believe though 2D data carries abundant information about human actions, 3D human carries relatively more geometric information about human bodies. In our tests, we also find that they are complementary to each other. In the future, we believe that 3D action understanding would be a more and more important direction. Moreover, 3D action/motion generation attracts more and more attention recently too. Currently, we do not use the face and hand detection and reconstruction of 3D humans for simplicity. We can use a more advanced but also heavier whole body detection and 3D reconstruction model such as SMPLify-X [137], to pursue better performance on face-hands related actions such as *eat*, *talk*, *grasp*, *etc*. We leave this to future work.

**Difference between CLIP-like Models and Ours.** Action understanding has a long story but the semantic space is usually defined without guidance, *e.g.*, selecting action classes according to the research interests or application requirements. Thus, different datasets cannot be directly used by other domains due to the action class setting divergence and semantic gap. This inhibits the development of general and open action understanding. Recently, CLIP [11] is proposed to utilize the flexible language prompt to encode the class labels, thus can bypass the class setting to achieve open-vocabulary training. But action semantics have their unique property overlooked by the intuitive visual-language alignment. In detail, verbs usually have many senses under different contexts and scenes. Moreover, verb taxonomy is hierarchical and different datasets usually adopt verbs in different granularities making the directly visual-language alignment difficult to capture the subtle semantics of actions. Directly using the label texts without any guidance is inefficient and hard to scale for future large-scale applications. Recent works also find that CLIP-style works usually perform not as open as we thought since the confusion of competing text features [138]. In our experiments, we also find that the ambiguity and complexity of action verbs and the obvious multi-label property of active persons hinder the effectiveness of CLIP a lot. In contrast, our structured semantic space design is explicit, well-designed to alleviate ambiguity, and related the similar verbs thanks to the linguistic knowledge from VerbNet. Thus, our model performs much better than the vanilla CLIP design on large-scale action learning tasks while showing great generalization ability, openness, and extensibility [138]. Besides the

unity and broad coverage, an extra benefit of our semantic space is that, though all the data would be placed in our verb tree, different users or researchers can only care about a part of the tree and do not need to process all the data of all the nodes while keeping the semantic structure knowledge.

**Weakly-Supervised Learning.** In our *Pangea*, due to the costly full annotation of the whole verb tree for all samples, we adopt a weakly-supervised way to train the models. In the future, we can annotate more verb nodes for more action classes from existing datasets, supplement more node labels for the existing samples, or utilize the self-supervised learning method designed for the typical positive unlabeled setting (PU, only some of the positive samples have labels) [139] to further advance our weakly-supervised system.

**Long-tailed Distribution.** Though we collect a lot of data in *Pangea*, the distribution is still long-tailed due to the natural data distribution. However, in the future, the community can easily collect data for the rare nodes and train a more versatile model covering more nodes and study more on how to generate better pseudo labels according to the language structure knowledge.